January 27, 2011

Revised March 15

ClC-7 is a slowly voltage-gated $2Cl^-/1H^+$-exchanger and requires Ostm1 for transport activity

Lilia Leisle[*], Carmen F. Ludwig[*], Florian A. Wagner,
Thomas J. Jentsch[§], Tobias Stauber

Leibniz-Institut für Molekulare Pharmakologie (FMP) and Max-Delbrück-Centrum für Molekulare Medizin (MDC), Robert-Rössle-Str. 10, 13125 Berlin, Germany

[*]Equal contribution

[§]Corresponding author
e-mail: Jentsch@fmp-berlin.de
Phone: +49-30-9406-2961
Fax: +49-30-9406-2960

Running title: Slowly voltage-gated 2Cl/H exchange by ClC-7/Ostm1

character count: 48,929

ABSTRACT

Mutations in the ClC-7/Ostm1 ion transporter lead to osteopetrosis and lysosomal storage disease. Its lysosomal localization hitherto precluded detailed functional characterization. Using a mutated ClC-7 that reaches the plasma membrane, we now show that both the amino-terminus and transmembrane span of the Ostm1 β-subunit are required for ClC-7 Cl^-/H^+-exchange, whereas the Ostm1 transmembrane domain suffices for its ClC-7-dependent trafficking to lysosomes. ClC-7/Ostm1 currents were strongly outwardly rectifying owing to slow gating of ion exchange which itself displays an intrinsically almost linear voltage-dependence. Reversal potentials of tail currents revealed a $2Cl^-/1H^+$ exchange stoichiometry. Several disease-causing *CLCN7* mutations accelerated gating. Such mutations cluster to the second cytosolic CBS domain and potential contact sites at the transmembrane segment. Our work suggests that gating underlies the rectification of all endosomal/lysosomal CLCs and extends the concept of voltage-gating beyond channels to ion exchangers.

Key words: chloride channel / trafficking / structure-function / antiport / conductance

CLC anion transport proteins (Jentsch, 2008), first identified by the cloning of the Cl^--channel ClC-0 from *Torpedo* (Jentsch *et al*, 1990), associate to dimers of identical or closely related subunits. Each CLC subunit contains an ion translocation pathway that is largely independent from the other subunit (Dutzler *et al*, 2002; Lorenz *et al*, 1996; Ludewig *et al*, 1996; Middleton *et al*, 1996; Robertson *et al*, 2010; Weinreich & Jentsch, 2001). Some CLC channels, however, display 'common gating' of both pores (Accardi & Pusch, 2000; Bauer *et al*, 1991; Miller & White, 1984). Eukaryotic CLC proteins have large cytosolic carboxyterminal domains comprising two CBS (cystathionine-β-synthase) domains that in some cases can bind nucleotides like ATP (Meyer *et al*, 2007) and have a poorly understood role in gating (Bykova *et al*, 2006; Estévez *et al*,

2004; Fong *et al*, 1998; Zhang *et al*, 2008; Zifarelli & Pusch, 2009b). Crystal structures of bacterial (Dutzler *et al*, 2002) and algal (Feng *et al*, 2010) CLC proteins, and of CBS domains from vertebrate CLCs (Markovic & Dutzler, 2007; Meyer & Dutzler, 2006; Meyer *et al*, 2007), have yielded important insights on how their structure relates to their biophysical properties.

Intriguingly, the CLC gene family comprises both Cl^- channels and electrogenic Cl^-/H^+-exchangers (Jentsch, 2008). The border between these different transport classes, however, is blurred, as gating of the ClC-0 Cl^- channel may involve the transport of a proton (Lisal & Maduke, 2008) and because certain anions can uncouple anion flux from proton countertransport (Bergsdorf *et al*, 2009; Nguitragool & Miller, 2006; Zdebik *et al*, 2008; Zifarelli & Pusch, 2009a). Moreover, transport activity of mammalian ClC-3 to ClC-6 Cl^-/H^+-exchangers is strongly voltage-dependent (Friedrich *et al*, 1999; Li *et al*, 2002; Neagoe *et al*, 2010; Steinmeyer *et al*, 1995). Their almost instantaneous deactivation at negative voltages precludes measurements of tail currents and it remains unresolved whether their voltage-dependence results from a voltage-sensitivity of the exchange process *per se* or from turning the transporter 'on' and 'off' ('gating') (Hebeisen *et al*, 2003; Picollo *et al*, 2010; Smith & Lippiat, 2010; Zdebik *et al*, 2008).

Mammalian endosomal/lysosomal Cl^-/H^+-exchangers (ClC-3 to ClC-7) regulate vesicular H^+ and Cl^- concentration (Jentsch, 2007; Novarino *et al*, 2010; Weinert *et al*, 2010). Disruption of endosomal ClC-5 impairs renal endocytosis (Piwon *et al*, 2000) in Dent's disease (Lloyd *et al*, 1996), whereas mutations in lysosomal ClC-7 entail osteopetrosis and lysosomal storage disease (Kasper *et al*, 2005; Kornak *et al*, 2001). Similar phenotypes were observed when uncoupling point mutations converted these exchangers into pure anion conductors (Novarino *et al*, 2010; Weinert *et al*, 2010). ClC-7 needs Ostm1 as β-subunit for protein stability (Lange *et al*, 2006). Hence disruption of Ostm1 results in osteopetrosis (Chalhoub *et al*, 2003) and lysosomal pathology (Lange *et al*, 2006; Pressey *et al*, 2010) just like a loss of ClC-7. It has remained unclear which parts of Ostm1

interact with ClC-7 and whether Ostm1 not only stabilizes ClC-7, but also modulates its ion transport activity.

Apart from the acid-secreting membrane of osteoclasts (Kornak *et al*, 2001; Lange *et al*, 2006), ClC-7/Ostm1 is absent from the plasma membrane, severely limiting its biophysical characterization. Transport studies of native lysosomes (Graves *et al*, 2008; Weinert *et al*, 2010) suggest that ClC-7 mediates Cl^-/H^+-exchange. However, no currents could be measured, essential properties like voltage-dependence, kinetics and substrate specificity have remained unknown, and no structure-function analysis could be performed. Here we exploit the partial plasma membrane expression of recently described ClC-7 mutants which disrupted cytosolic sorting motifs (Stauber & Jentsch, 2010) to characterize the biophysical properties of ClC-7 and its functional interaction with Ostm1. The slow deactivation of ClC-7/Ostm1 resulted in tail currents that revealed functional features that could not be studied with other CLC anion/proton exchangers.

RESULTS

Basic characterization of ClC-7/Ostm1 Cl^-/H^+-exchange

Disrupting two dileucine lysosomal sorting motifs in the cytosolic N-terminus of rat ClC-7 (rClC-7) partially redirects the mutant protein (rClC-$7^{LL23/24AA,LL36/37AA}$, in short rClC-7^{PM}) to the plasma membrane (Stauber & Jentsch, 2010). Likewise human ClC-7 (hClC-7) carrying the mutations LL23/24AA and LL68/69AA (hClC-7^{PM}) partially traffics to the plasma membrane, as ascertained in a chemiluminescence assay for an added extracytosolic HA-tag (Figure 1A). This assay failed to detect hClC-7^{PM} when co-expressed with Ostm1, possibly owing to a shielding of the epitope by the highly glycosylated N-terminus of Ostm1 (Lange *et al*, 2006). Indeed, both rClC-7^{PM}/Ostm1 and hClC-7^{PM}/Ostm1 gave robust plasma membrane currents (Figure 1B,C for rClC-7^{PM}, and Supplementary Figure S1A for hClC-7^{PM}). Since currents of human and rat ClC-7^{PM} were indistinguishable in both *Xenopus* oocytes and transfected mammalian cells, we refer to both as ClC-7^{PM} in the following.

Expression of ClC-7^{PM}/Ostm1 in *Xenopus* oocytes (Figure 1B,C and Supplementary Figure S1A), tsA201 or HeLa cells (Supplementary Figure S1B) yielded strongly outwardly rectifying currents that activated slowly at voltages more positive than ~ +20 mV. In stark contrast to ClC-3 through ClC-6 (Friedrich *et al*, 1999; Li *et al*, 2002; Matsuda *et al*, 2008; Neagoe *et al*, 2010), full activation was not even observed after several seconds and slow deactivation resulted in tail currents at negative voltages (Figure 1C (arrow) and Supplementary Figure S1A,B). Whole-cell patch-clamp experiments in HeLa cells showed that ClC-7^{PM}/Ostm1 currents do not require intracellular ATP (Supplementary Figure S1C). We neither observed significant changes in current amplitudes like described for ClC-5 (Zifarelli & Pusch, 2009b) which is known to bind ATP by its CBS domains (Meyer *et al*, 2007), nor changes in voltage-dependence.

As typical for CLC antiporters (Bergsdorf *et al*, 2009; Dutzler *et al*, 2003; Friedrich *et al*, 1999; Li *et al*, 2002; Neagoe *et al*, 2010; Picollo & Pusch, 2005; Scheel *et al*, 2005; Zdebik *et al*, 2008), mutating the 'gating glutamate' (E245 in rat) of ClC-7^{PM} to alanine resulted in almost ohmic, time-independent currents,

and changing the 'proton glutamate' (E312 in rat) to alanine reduced currents to background levels (Figure 1B,C and Supplementary Figure S1A). ClC-7^{PM}/Ostm1 mediated Cl^-/H^+-exchange as evident from depolarization-induced intracellular alkalinization of *Xenopus* oocytes expressing these proteins (Figure 1D). In these 'Fluorocyte' experiments, the pH-dependent fluorescence of BCECF previously injected into oocytes provides a semi-quantitative measure of cytosolic pH changes in response to depolarizing voltage-steps. Depolarization not only activates ClC-7^{PM}/Ostm1, but also provides a driving force for coupled H^+-exit/Cl^--entry. Outward transport of protons required extracellular Cl^- (Figure 1E), could occur against its electrochemical gradient (pH_o=5.5, Figure 1E), and was abolished by either the E245A or the E312A mutation (Figure 1D). ClC-7^{PM}/Ostm1 currents decreased upon replacing extracellular Cl^- by I^-, but unlike ClC-4 and -5 (Friedrich *et al*, 1999), currents were not larger with NO_3^- (Figure 2A). Replacing a Cl^--coordinating serine by proline (rClC-7(S202P)) increased the nitrate/chloride conductance ratio as with other CLC antiporters (Bergsdorf *et al*, 2009; Neagoe *et al*, 2010; Zifarelli & Pusch, 2009a) and with ClC-0 (Bergsdorf *et al*, 2009; Picollo *et al*, 2009). Akin to ClC-4, -5 and -6 (Friedrich *et al*, 1999; Neagoe *et al*, 2010; Picollo *et al*, 2010), currents were decreased by acidic extracellular pH (Figure 2B). In addition to a diminished driving force for Cl^-/H^+-exchange with increased extracellular $[H^+]$, faster activation kinetics at more alkaline pH_o contributes to the pH-dependence of ClC-7^{PM}/Ostm1 outward currents (Figure 2C). Voltage-dependent current activation was also strongly dependent on temperature (Figure 2D). Mono-exponential fits yielded activation rate constants of 2.8 ± 0.2 s^{-1} at 21°C and 16.6 ± 1.9 s^{-1} at 37°C, giving an estimate of $Q_{10} \approx 3$.

Slow ClC-7/Ostm1 gating allows characterization of an 'open exchanger'

The slow deactivation of ClC-7^{PM}/Ostm1 currents provides a unique opportunity to study mammalian Cl^-/H^+-exchange at negative membrane voltages. Using protocols developed for ion channels, we activated ('opened') ClC-7^{PM}/Ostm1 by positive prepulses and measured tail currents from transfected HeLa cells at

different test voltages (Figure 3A). We increased tail current amplitudes by including 121 mM Cl^- in the patch pipette. Tail currents were extrapolated to the beginning of the test pulse to obtain the voltage-dependence of 'open exchanger' currents (Figure 3A). Contrasting with the strong voltage dependence of pseudo-steady-state currents, 'open exchanger' currents displayed only very slight outward rectification.

Whereas the strong rectification and near-instantaneous deactivation of ClC-4 and ClC-5 precludes measurements of reversal potentials (Friedrich *et al*, 1999; Steinmeyer *et al*, 1995), ClC-7^{PM}/Ostm1 tail currents allowed us to determine Cl^-/H^+-coupling ratios from Cl^-- and H^+-dependent shifts in reversal potentials (Figure 3B). Our results were best fitted by a $2Cl^-:1H^+$ stoichiometry. The apparent deviation from this stoichiometry at nominal pH_o of 8.4 might be explained by depolarization-induced outward transport of protons through the exchanger (Zifarelli & Pusch, 2009a). This process is expected to cause a larger deviation of actual from nominal pH at the lower H^+-concentrations of more alkaline pH.

Whereas the tail current analysis of instantaneous 'open exchanger' currents requires the same open probability p_{open} at the beginning of test pulses (as indicated above by identical macroscopic currents), p_{open} must have reached steady-state at the respective voltage when p_{open} is determined as a function of voltage by tail currents. The slow voltage-dependent activation of ClC-7^{PM}/Ostm1, however, precluded reliable measurements of steady-state currents that are needed for this analysis. We therefore resorted to a ClC-7 point mutant (R762Q; described below) that drastically accelerates activation. ClC-7^{PM}(R762Q)/Ostm1 currents reached steady-state already ~400 ms after the beginning of voltage steps (Figure 3C). At t = 500 ms, tail currents were measured at a constant test voltage (+80 mV) as function of the voltage of the preceding pulse (between -40 and +140 mV). After correcting for endogenous HeLa cell currents, apparent $p_{open}(V)$ was obtained by extrapolating tail currents to the time of the voltage step (see Methods). Boltzmann fits (Figure 3D) revealed a voltage of half-maximal activation $V_{½} \approx 82$ mV and an apparent gating charge of $z_n \approx 1.32$. Although we

performed this tail analysis study with a mutant, we expect the values of 'WT' ClC-7/Ostm1 to be similar.

Structural basis and functional consequences of Ostm1-ClC-7 interactions

So far, all experiments on ClC-7^{PM} were performed in co-expression with Ostm1. When we expressed ClC-7^{PM} with or without Ostm1 in HeLa cells (Supplementary Figure S1D) or *Xenopus* oocytes (not shown), ClC-7^{PM} yielded currents only together with Ostm1. Since ClC-7^{PM} clearly reaches the plasma membrane also without Ostm1 (Figure 1A and (Stauber & Jentsch, 2010)), these results indicate that Ostm1 is needed to activate ClC-7 ion transport.

We next asked which parts of Ostm1 interact with ClC-7. We constructed chimeras with CD4, a protein that shares the type I transmembrane topology of Ostm1 (Lange *et al*, 2006) but traffics to the plasma membrane by default. The extracellular, transmembrane, and intracellular domains of Ostm1 were replaced by those of CD4 either individually or in combination. Without ClC-7, Ostm1 stays in the endoplasmic reticulum (ER), whereas a portion of Ostm1 reaches lysosomes upon co-expression with ClC-7 (Lange *et al*, 2006). We first ascertained that Ostm1 and Ostm1/CD4 chimeras carrying C-terminal GFP-tags were confined to the ER and/or plasma membrane of transfected HeLa cells (Figure 4A). We then co-transfected GFP-tagged Ostm1/CD4 chimeras with ClC-7 and assayed the co-localization of GFP fluorescence with the lysosomal marker LAMP-1 as read-out for Ostm1-ClC-7 interaction (Figure 4B,C and Supplementary Figure S2). The transmembrane domain (TMD) of Ostm1 was necessary and sufficient for Ostm1 constructs being carried to lysosomes by ClC-7 (Figure 4C).

While these experiments suggested that the TMD of Ostm1 binds ClC-7, other parts of Ostm1 may modulate ClC-7 transport activity. We therefore assayed currents of *Xenopus* oocytes co-expressing ClC-7^{PM} and Ostm1/CD4 chimeras (Figure 4D). As expected from our localization assay, currents were not detectable when the TMD of Ostm1 was replaced by that of CD4. Even larger currents were observed when ClC-7^{PM} was co-expressed with a chimera (OOC)

in which the Ostm1 C-terminus was replaced by that of CD4. By contrast, currents were indistinguishable from background with chimeras lacking the Ostm1 N-terminus (Figure 4D), even though ClC-7^{PM} was still able to reach the plasma membrane (Supplementary Figure S3). Hence both the N-terminus and TMD of Ostm1 are required for ClC-7 transport activity.

Functional effects of human *CLCN7* mutations underlying osteopetrosis

The plasma membrane expression of ClC-7^{PM}/Ostm1 allowed us for the first time to study functional consequences of disease-causing *CLCN7* mutations (Cleiren *et al*, 2001; Frattini *et al*, 2003; Kornak *et al*, 2001; Letizia *et al*, 2004; Pangrazio *et al*, 2010; Phadke *et al*, 2010; Waguespack *et al*, 2003), which we selected from different categories based on the mode of inheritance (recessive vs. dominant) and on their location within the protein (transmembrane region or cytoplasmic CBS domain) (Figure 5A and Supplementary Figure S4).

Within all *CLCN7* mutation categories mentioned above we found mutations that abolished or strongly reduced currents (Figure 5C and Supplementary Figure S5A). Surprisingly, other mutations either left ClC-7^{PM} currents virtually unchanged (e.g. S744F (Frattini *et al*, 2003)) or accelerated their activation kinetics between moderately (e.g. the frameshift mutation G796fs (Cleiren *et al*, 2001)) and dramatically (e.g. R762Q (Kornak *et al*, 2001)) (Figure 5C, Supplementary Figure S5A). Mutants that yielded plasma membrane currents also transported H^+ as revealed by Fluorocyte (Zdebik *et al*, 2008) experiments (not shown). To test whether changed subcellular targeting of ClC-7/Ostm1 might explain the disease-causing effect of those mutants, we inserted them into hClC-7 instead of hClC-7^{PM} and co-expressed them with GFP-tagged Ostm1 in HeLa cells. However, in addition to a pronounced ER-like labelling, all mutants that gave currents (in hClC-7^{PM}) reached their normal destination (lysosomes) where they co-localized with Ostm1 (Figure 5D and Supplementary Figure S5B). Only three of the mutants with reduced currents were retained in the ER, whereas the other six partially localized with Ostm1 to late endosomes/lysosomes (Figure 5D

and Supplementary Figure S5B). In the absence of lysosomal targeting sequences, ClC-7 reaches the plasma membrane by default once it has left the ER (Stauber & Jentsch, 2010). Hence normal lysosomal targeting (in hClC-7) of the V297M, F318L, L490F, L651P, R767P and R767W mutants, all of which reduce or abolish plasma membrane currents in hClC-7^{PM}, suggests that these mutations may interfere directly with the ion transport of ClC-7 or with the mechanism by which Ostm1 activates ClC-7. One should note, however, that all these mutants were able to carry Ostm1 to lysosomes. A reduction in the expression level due to limited stability may also contribute to reduced currents. Western blot analysis showed that this was not the case for the V297M and F318L mutants, whereas protein levels were markedly reduced with the L490F mutant (Supplementary Figure S6).

DISCUSSION

Despite the medical importance of ClC-7/Ostm1 and its crucial role in lysosomal function (Kasper *et al*, 2005; Kornak *et al*, 2001; Lange *et al*, 2006; Wartosch *et al*, 2009; Weinert *et al*, 2010), the only available information concerning its biophysical properties has remained its ability to perform Cl^-/H^+-exchange (Graves *et al*, 2008; Weinert *et al*, 2010). Acid-activated currents previously ascribed to ClC-7 (Diewald *et al*, 2002) most likely represent currents endogenous to the expression systems (Jentsch, 2008). Exploiting the partial plasma membrane localization of ClC-7 mutants which we have recently described (Stauber & Jentsch, 2010), we could now study for the first time important details of ion transport properties, investigate effects of human disease-causing mutations, and show that ClC-7 needs specific domains of the Ostm1 β-subunit not only for protein stability (Lange *et al*, 2006), but also for ion transport activity.

Voltage-gating of intrinsically linear voltage-dependent $2Cl^-/H^+$-exchange

Several properties of ClC-7/Ostm1 described here have recently emerged as being typical for mammalian CLC exchangers (Jentsch, 2008). This includes the preference of Cl^- over I^-, decreased transport activity with acidic external pH, strong outward rectification, and effects of neutralizing 'gating' and 'proton' glutamates which result in an uncoupling of anion movement from protons and an apparent abrogation of all ion transport, respectively.

While ClC-7/Ostm1 differs from ClC-3 to -6 with respect to NO_3^- selectivity, the most important biophysical difference to those transporters is the slow voltage-dependent activation and deactivation of ClC-7/Ostm1. Whereas ClC-4 and -5 show a similarly steep voltage-dependence with significant currents being observable only at positive voltages, a major component of the current activated upon depolarization appears instantaneous, with the remaining <30% reaching steady-state in less than ~100 ms (Friedrich *et al*, 1999; Steinmeyer *et al*, 1995). Despite the drastic difference in gating kinetics, the $V_{½}$ of ClC-7^{PM}(R762Q)/Ostm1 (~82 mV) agrees well with that of ClC-4 measured in the presence of uncoupling anions (Orhan *et al*, 2011). Most importantly, currents of ClC-4 and ClC-5 deactivated almost instantaneously at negative voltages, with no tail currents being detectable (Friedrich *et al*, 1999; Steinmeyer *et al*, 1995). Therefore, it was impossible to determine whether their Cl^-/H^+-exchange can function, in principle, also at negative voltages (i.e. lumen-positive for vesicles).

ClC-7/Ostm1 currents, by contrast, did not reach steady-state even after more than 2 seconds. We have avoided using longer pulses to minimize confounding local changes in Cl^-- and H^+-concentrations. Although deactivation upon stepping back to negative potentials was faster than activation, it resulted in respectable tail currents, in particular when $[Cl^-]_i$ was kept high in whole-cell patch-clamp measurements. Currents at negative voltages clearly demonstrated that net Cl^-/H^+-exchange can occur in both directions, which has not been demonstrated previously for any mammalian CLC. Instantaneous tail currents displayed an almost linear dependence on voltage. As their slight outward rectification might be owed to the difference in $[H^+]$ and $[Cl^-]$ on both sides of the membrane, we

propose that the intrinsic Cl^-/H^+-exchange rate is nearly linearly related to the driving force. This hypothesis needs to be tested in future studies under a broader range of conditions. The almost ohmic tail currents also indicate that the model of (Zdebik *et al*, 2008), in which the voltage-dependence of ClC-5 may be related to a voltage-driven transport of cytosolic H^+ to the central exchange site, does not apply for ClC-7/Ostm1. It has also been questioned for ClC-5 (Picollo *et al*, 2010).

We conclude that voltage-dependence of ClC-7/Ostm1 is almost exclusively caused by a slow activation/deactivation process that we like to refer to as 'gating' in analogy to the terminology used for ion channels. CLC Cl^- channels have two kinds of gates, one for each pore of the (homo)dimeric channel (the 'protopore gate', which relates to the 'gating glutamate'), and a less well understood 'common gate' that acts on both pores simultaneously (Jentsch, 2008). In the *Torpedo* channel ClC-0, the protopore gate is fast and has a Q_{10} of ~2.2, whereas the common gate is slow with a Q_{10} of ~40 (Pusch *et al*, 1997). However, protopore and common gates of the mammalian muscle Cl^- channel ClC-1 display Q_{10} values of ~3 and ~4, respectively (Bennetts *et al*, 2001). Therefore, the Q_{10} of ClC-7/Ostm1 activation cannot serve as criterion for deciding whether the underlying process is analogous to protopore or common gating.

The majority of those human *CLCN7* mutations found to accelerate the 'gating' of ClC-7/Ostm1 affect residues in the ClC-7 C-terminus. Two of these residues (R762 and R767) are located at the surface of the second CBS domain in close proximity to the transmembrane part as revealed by the X-ray structure of algal CmClC (Feng *et al*, 2010). Intriguingly, two other 'accelerating' mutations (L213F and R286Q) affect residues in the membrane part which are in close proximity to CBS2 (Figure 5B and Supplementary Video 1).

Hence the slow gating of ClC-7/Ostm1 may involve interactions of CBS2 with the transmembrane part of ClC-7. As the cytoplasmic C-termini were implicated in 'common gating' of ClC-0 (Bykova *et al*, 2006; Estévez *et al*, 2004; Fong *et al*,

1998), these observations indirectly suggest that ClC-7/Ostm1 activity is regulated by a 'common gate'.

Voltage-dependence was abolished by the uncoupling mutation E245A as in other CLC transporters (Bergsdorf *et al*, 2009; Friedrich *et al*, 1999; Neagoe *et al*, 2010; Picollo & Pusch, 2005; Scheel *et al*, 2005). This result is compatible with the notion that E245, which may change its position during $2Cl^-/H^+$-exchange cycles (Feng *et al*, 2010), acts as a 'gate'. The short distance which its negative side chain may move in the electric field, however, seems to exclude a function as voltage-sensor as it would result in an apparent 'gating charge' much smaller than 1. The apparent gating valence determined here for ClC-7^{PM}(R762Q)/Ostm1 ($z_n \approx 1.32$) agrees well with that of ClC-4 in the presence of uncoupling anions (Orhan *et al*, 2011) and with gating charges determined for ClC-0 (Bauer *et al*, 1991; Hanke & Miller, 1983; Pusch *et al*, 1995), ClC-1 (Pusch *et al*, 1994) and ClC-2 (de Santiago *et al*, 2005) Cl^- channels. We envisage a conformational change, possibly involving cytosolic CBS domains, that fixes the position of E245 'gating glutamate', thereby resulting in a 'closed state' of the transporter. Whether the 'gating charge' is supplied by permeant ions (Lisal & Maduke, 2008; Pusch *et al*, 1995), intrinsic charges of the protein, or a combination thereof (Smith & Lippiat, 2010), remains an open question.

The tail currents of ClC-7/Ostm1 provided the unique possibility to determine the Cl^-/H^+-exchange stoichiometry from reversal potentials. These cannot be measured reliably with other endosomal/lysosomal CLC exchangers. Our data were best fit by a $2Cl^-:1H^+$ stoichiometry as originally described for the prokaryotic EcClC-1 (Accardi & Miller, 2004) and which might be rationalized in terms of a switch in the position of the 'gating glutamate' (Feng *et al*, 2010).

It is intriguing that ClC-7/Ostm1, just like the other vesicular CLC Cl^-/H^+-exchangers (Friedrich *et al*, 1999; Li *et al*, 2002; Neagoe *et al*, 2010; Steinmeyer *et al*, 1995), displays such strong voltage dependence. This rectification is not an inevitable consequence of the Cl^-/H^+-exchange *per se*, as our measurements of 'open transporter' currents have shown. This suggests that the rectification might have a physiological importance, which, however, remains obscure. The strong

outward rectification of ClC-4 and -5 has puzzled the field for a long time because it implies that these transporters are almost inactive in inside-positive endosomes (Jentsch, 2007; Jentsch *et al*, 2002). However, recent model calculations showed that vesicles may attain an inside-negative voltage through the activity of $2Cl^-/H^+$-exchangers (Weinert *et al*, 2010).

Transmembrane domain and exoplasmic N-terminus of Ostm1 are needed for ClC-7 ion transport activity

ClC-7 is the only CLC exchanger known to need an accessory subunit (Lange *et al*, 2006). This β-subunit, Ostm1, is a small type I transmembrane protein with a highly glycosylated N-terminus (Lange *et al*, 2006) that was identified as being truncated in the osteopetrotic *grey lethal* mouse (Chalhoub *et al*, 2003). The pathology resulting from a loss of Ostm1 was explained by the concomitant loss of ClC-7 which is unstable without its β-subunit (Lange *et al*, 2006). Our work now shows that Ostm1 is also needed for the ion transport activity of ClC-7. Hence the low levels of ClC-7 (~5% of WT protein) remaining in tissues of *Ostm1*$^{-/-}$ mice (Lange *et al*, 2006) are non-functional. Disruption of Ostm1 leads to a complete loss of ClC-7 ion transport.

To elucidate which parts of Ostm1 interact with ClC-7, we assayed the ClC-7-dependent trafficking of Ostm1 to lysosomes, an assay that turned out to be more reliable than co-immunoprecipitation (Lange *et al*, 2006). The single TMD of Ostm1 was necessary and sufficient for correct trafficking, suggesting that Ostm1-ClC-7 binding involves interactions between transmembrane helices of both ClC-7 and Ostm1. Consistent with the lack of interaction in the trafficking assay, a chimera in which the Ostm1 TMD was replaced by that of CD4 failed to activate ClC-7^{PM} ion transport. Surprisingly, ClC-7^{PM} transport activity also required the highly glycosylated extracytosolic aminoterminus of Ostm1. Normally Ostm1 is cleaved proteolytically in (or on its way to) lysosomes, but the cleavage products are still bound together by disulfide bonds (Lange *et al*, 2006). Since it is unlikely that ClC-7^{PM}/Ostm1 reaches the plasma membrane through a prelysosomal/lysosomal compartment, our results provide circumstantial

evidence that cleavage of Ostm1 is not needed for its ability to stimulate ion transport of ClC-7. The cytosolic C-terminus of Ostm1 was not needed, although we cannot exclude that it modulates ClC-7 transport as hinted at by the larger currents induced by the OOC chimera. Barttin, a protein that only interacts with ClC-K Cl^- channels (Estévez *et al*, 2001), is the only other β-subunit of CLC proteins known to date. Like Ostm1, barttin is thought to bind to ClC-K α-subunits through its transmembrane domains (Scholl *et al*, 2006; Tajima *et al*, 2007), but activation of ion transport requires its intracellular carboxy-terminus (Scholl *et al*, 2006).

Effects of disease-causing *CLCN7* mutations

Roughly forty different mutations in *CLCN7* have been found in humans suffering from osteopetrosis, from which we have selected 18 for the present analysis. No consistent differences concerning their effects on ion transport or trafficking were found when comparing recessive and dominant, or membrane- and CBS-domain localized mutations. As expected, several mutants yielded reduced currents, and in others voltage-activated currents were not detectable. G240R, G521R and R526W, all of which alter charges in a transmembrane domain, led to retention in the ER irrespective of co-expression with Ostm1. Like previously reported for the G215R mutant (Schulz *et al*, 2010), however, some mutants overcame ER retention when co-expressed with Ostm1 (data not shown). Several mutations reduced or abolished currents although normal lysosomal targeting (when inserted into hClC-7/Ostm1) indirectly indicated that they reached the plasma membrane in hClC-7^{PM}/Ostm1.

Surprisingly, half of the disease-causing mutations gave currents when studied in ClC-7^{PM}/Ostm1. In many cases these currents showed accelerated kinetics of activation, such as L213F, R286Q, R762Q, R762L, and R767Q. When expressed in HeLa cells together with Ostm1, these mutants (in hClC-7) could reach lysosomes. This raises the question whether the slow activation kinetics of ClC-7/Ostm1 is needed for its physiological function. However, trafficking and protein stability might be different *in vivo* as compared to heterologous

overexpression. Indeed, Western blots and immunofluorescence previously failed to detect ClC-7 protein in fibroblasts from a patient heterozygous for an early stop codon in *CLCN7* and the 'accelerating' R762Q mutation (Kornak *et al*, 2001).

Conclusions and outlook

While ClC-7 shares many biophysical properties with the other mammalian CLC Cl^-/H^+-exchangers, it is unique in that it needs a β-subunit (Ostm1) and that its activation and inactivation by voltage is much slower.

Whereas an interaction through transmembrane domains, as observed here for ClC-7/Ostm1, is not without precedent (Scholl *et al*, 2006; Tajima *et al*, 2007), the apparently strict dependence of ion transport activity on the highly glycosylated Ostm1 N-terminus (Lange *et al*, 2006) is surprising. It raises the question whether sugar moieties on Ostm1 interact with the rather limited extracytosolic part of the ClC-7 protein and how this activates ion transport. This activation might involve the same gating mechanism that 'opens' and 'closes' ClC-7/Ostm1 like an ion channel – the difference being that it is not a purely diffusive pore, but ion exchange which is 'gated'. It is intriguing that ClC-7/Ostm1 is the only endosomal/lysosomal CLC which is gated so slowly and that several disease-causing missense mutations in the ClC-7 CBS2 domain accelerate its activation. Interestingly, there is not even one missense mutation in a CBS domain among the many *CLCN5* mutations identified so far in Dent's disease (Jentsch, 2008; Lloyd *et al*, 1996). Together with the fact that ClC-5 activates and deactivates much faster, these observations suggest that the sluggish voltage-dependence of ClC-7/Ostm1 might play a physiological role. This seems surprising in view of its localization to the non-excitable membranes of lysosomes and the osteoclast ruffled border, but abrupt voltage-changes that would not significantly 'open' ClC-7/Ostm1 seem possible – for instance, in second-messenger induced release of Ca^{++} from lysosomes.

Acknowledgements

We thank Janet Liebold, Nicole Krönke, Patrick Seidler and Silke Zillmann for technical assistance, Anselm A. Zdebik for discussions, Andrew J. Plested for critical reading of the manuscript, and Pawel Fidzinski for advice on patch-clamping. This work was supported, in part, by the Deutsche Forschungsgemeinschaft (JE 164/7).

Author contributions

The study was conceived and designed by TJJ and TS, with contributions of LL and CFL. TS generated constructs, and investigated expression, trafficking and localization of mutants. LL and CFL performed electrophysiological experiments and FAW trafficking studies to determine ClC-7/Ostm1 interactions. LL, CFL, TJJ and TS analyzed the data. TJJ and TS wrote the paper, with contributions of LL and CFL.

FIGURE LEGENDS

Figure 1 Basic characterization of ClC-7^{PM}/Ostm1 in *Xenopus* oocytes. (**A**) Chemiluminescence assay for surface detection of hClC-7 and hClC-7^{PM} with an extra-cytosolic HA-tag. hClC-7^{PM}-exHA, but not hClC-7-exHA is detected at the surface of *Xenopus* oocytes. Co-expression with Ostm1 suppresses the luminescence signal although ClC-7^{PM}/Ostm1 yields plasma membrane currents (in B,C). Mean luminescence intensity (error bars, s.e.m.) normalized to hClC-7^{PM}-exHA from 4 independent experiments. (**B, C**) Two-electrode voltage-clamp analysis in *Xenopus* oocytes. Representative voltage-clamp traces (C) of rClC-7^{PM} ('WT'), rClC-7^{PM}(E245A) and rClC-7^{PM}(E312A) co-expressed with Ostm1. Arrow indicates tail currents. Voltage was clamped from -80 to +80 mV in 2-sec steps of 20 mV (inset). Mean ± s.e.m. of currents reached after 2 sec plotted (B) as function of voltage (rClC-7^{PM}, n=20; rClC-7^{PM}(E245A), n=13; rClC-7^{PM}(E312A), n=11; uninjected, n=16 oocytes from at least 3 batches). Virtually identical results were obtained with hClC-7^{PM} (Supplementary Figure 1A). (**D**, **E**) Intracellular pH changes of *Xenopus* oocytes co-expressing rClC-7^{PM} ('WT' or glutamate mutants) with Ostm1 in response to a 10-sec depolarization. *Top traces*, clamp currents; *bottom traces*, pH-dependent BCECF fluorescence measured with the Fluorocyte method (Zdebik *et al*, 2008). Increased fluorescence means alkalinization. Unless indicated otherwise, extracellular solution contained 96 mM Cl^- at pH 7.4. For 0 Cl^-, gluconate replaced Cl^-. Left traces in D and E are from the same oocyte, and center and right recording in E are from one oocyte as well. Similar results were obtained with at least 5 oocytes from 3 batches.

Figure 2 Modulation of ClC-7/Ostm1 by anions, protons and temperature. (**A**) Relative anion conductance of oocyte-expressed rClC-7^{PM}/Ostm1 in the presence of different extracellular anions (96 mM). Clamp protocol as in Figure 1C. Mean ± s.e.m. of currents reached after 2 s at +80 mV were normalized to the current in Cl^- for each oocyte (*white bars*) (Cl^-, n=32 oocytes; Br^-, n=7; NO_3^-, n=6; I^-, n=5; gluconate ($gluc^-$), n=5). G*ray bar,* NO_3^- conductance of rClC-

7^{PM}(S202P)/Ostm1 mutant measured and normalized as above (n=9). (**B**) Dependence of rClC-7^{PM}/Ostm1 currents on pH_o. I/V curves were obtained as in Figure 1B with currents normalized to those at pH_o=7.4 and 80 mV. ≥ 6 oocytes per data point. (**C**) *Left*, typical voltage-clamp traces (*top right*, protocol) obtained at different pH_o. Note different current scales that were chosen to normalize current amplitudes to the end of +80 mV pulse for better visualizing changes in activation kinetics. *Right*, τ was determined by single-exponential fit of the 80mV traces for ≥ 6 oocytes per pH value. Mean ± s.e.m. as function of pH_o. (**D**) Typical voltage-clamp traces of rClC-7^{PM}/Ostm1 (protocol as in C) at different temperatures, representative for 11 oocytes in which temperature was changed between 21°C to 29°C (n=8) and/or 37°C (n=9).

Figure 3 Tail current analysis of ClC-7^{PM}/Ostm1. (**A**) After activating HeLa cell-expressed rClC-7^{PM}/Ostm1 by pulses to +80 mV in whole-cell patch-clamp experiments, tail currents were measured at test voltages between -100 and +100 mV. *Left*, representative current traces (*inset*, clamp protocol). *Right*, I/V curve of 'open exchanger' obtained by extrapolation to the beginning of test pulses, shown together with 'pseudo-steady-state' currents measured after 2 s without preceding activation. Mean values ± s.e.m. normalized to the current at +80 mV of 8 ('open exchanger') and 19 ('pseudo-steady-state') cells. Error bars are mostly smaller than symbols. (**B**) Determination of nCl^-/H^+-exchange stoichiometry from reversal potentials of tail currents. HeLa cell-expressed rClC-7^{PM}/Ostm1 was clamped using a protocol as in A, but tail currents were measured at only three voltages close to reversal potentials (-20 to +20 mV, or 0 to +40 mV). The contribution of endogenous currents was estimated by short pulses from -80 to 0 mV before activating ClC-7^{PM}/Ostm1 (see Methods). $[Cl^-]_o$ was shifted from 139 to 39 and/or 19 mM Cl^- (*top*, representative traces from one cell) and pH_o from 7.4 to 6.4 and/or 8.4. *Bottom*, reversal potentials corrected for background currents and liquid-junction potentials. Crosses, individual measurements. Filled circles and error bars, mean ± s.d. Lines, predictions for an nCl^-/H^+-exchanger with n=1, 2 and 3, and for a Cl^--channel (1:0) under our

experimental conditions. Dashed lines in A and B, I=0. (**C**) Tail current analysis of hClC-7^{PM}(R762Q)/Ostm1 expressed in HeLa cells to determine $p_{open}(V)$. Clamp protocol at bottom. (**D**) Apparent open probability p_{open} as function of prepulse voltage, determined from tail currents as shown in (**C**). The line shows the fit by the Boltzman function $p_{open} = 1/(1 + \exp(z_n * e_0(V_{½} - V)/kT))$, which yielded z_n= 1.32 and $V_{½}$ = 82 mV. Values are mean of 5 experiments. Error bars, s.e.m.

Figure 4 Domains of Ostm1 that interact with ClC-7. (**A**) When transfected into HeLa cells, Ostm1-GFP localizes to the ER, CD4-GFP mostly to the plasma membrane, and a GFP-tagged CD4 chimera containing the TMD of Ostm1 (COC-GFP) to the ER and plasma membrane. (**B**) When co-transfected with HA-tagged rClC-7, Ostm1-GFP and COC-GFP, but not CD4-GFP, co-localized with rClC-7-HA (immuno-labelled for the HA epitope) to late endosomes/lysosomes (marked by immuno-labelling for LAMP-1). (**C**) Statistical analysis of lysosomal targeting of Ostm1, CD4 or chimeras thereof expressed either without (-) or with (+) rClC-7-HA assayed as in A and B. In the 3-letter abbreviations, C means CD4, O Ostm1, in the sequence extracytosolic N-terminal part, TMD, and cytoplasmic C-terminus. Means of 3-4 independent experiments with >100 cells each evaluated. Error bars, s.e.m. Constructs containing the TMD of Ostm1 localized to lysosomes upon co-expression with rClC-7. (**D**) Typical current traces of *Xenopus* oocytes co-expressing rClC-7^{PM} with Ostm1, CD4, or CD4/Ostm1 chimeras. Expression of significant currents required the presence of both the N-terminus and TMD of Ostm1. Similar results were obtained with at least 10 oocytes of at least 3 batches.

Figure 5 Characterization of osteopetrosis-causing mutations in human ClC-7. (**A**) Position of analyzed dominant and recessive osteopetrosis-causing mutations (solid and open stars, respectively) in a CLC topology model (Dutzler *et al*, 2002). Mutations yielding no currents shown in purple (when retained with Ostm1-GFP in the ER of HeLa cells) and red (when exported from the ER), those with apparently normal currents in green, and those with accelerated activation in

blue (see C, D and Supplementary Figure S5). (**B**) Close-up of X-ray structure of CmClC (Feng *et al*, 2010) displaying the location of ClC-7 residues that accelerate gating when mutated. Except for L213 (corresponding to L174 in CmClC), the depicted ClC-7 residues are not identical to those of CmClC at these positions (R286, P619, R762 and R767 of hClC-7 correspond to L241, R532, V680 and S685, respectively, in CmClC) (Feng *et al*, 2010). The transmembrane part of one subunit is shown in gray, CBS2 and the linker to CBS1 of that subunit in red and yellow, respectively. Green helices at left are from the second subunit of the homodimer. (**C**) Representative current traces of hClC-7^{PM} ('WT' or selected osteopetrosis-causing mutants) upon expression with Ostm1 in *Xenopus* oocytes. Mutants yielded either no or very low currents (R526W and L490F), apparently normal currents (S744F), or displayed accelerated activation (R762Q). (**D**) Subcellular localization of hClC-7 and selected mutants co-expressed with Ostm1-GFP in HeLa cells. Cells were immuno-labelled for hClC-7 and LAMP-2. In most cases, hClC-7 co-localized with Ostm1-GFP to LAMP-2-positive structures in addition to localizing to ER-like structures. However, hClC-7(R526W) remains with Ostm1-GFP in the ER (highlighted by nuclear envelope staining). In cells with a clear excess of Ostm1-GFP (asterisk), it predominantly localizes to the ER.

MATERIALS AND METHODS

Expression constructs and antibodies. For expression of untagged proteins in cell culture, constructs were subcloned into pcDNA3 or pcDNA3.1(+) (both Invitrogen). Constructs for rat ClC-7 in this vector have been described previously (Stauber & Jentsch, 2010). The construct for expression of fluorescently tagged Ostm1 in the pEGFP-N3 vector (Clontech) linking Ostm1 at the C-terminus with green fluorescent protein (GFP) by the sequence VDGTAGPGSIAT has been described (Stauber & Jentsch, 2010). To generate chimeric constructs between Ostm1 and CD4, the DNA sequences encoding the amino-terminal part (aa 1-286 for Ostm1 and aa 1-397 for CD4), the transmembrane region (estimated by hydrophobicity; aa 287-309 for Ostm1 and aa 398-420 for CD4) and the carboxy-terminal region (aa 310-338 for Ostm1 and aa 421-458 for CD4) of the respective protein were combined by recombinant PCR and cloned into pEGFP-N3.

Constructs for heterologous expression in *Xenopus* oocytes were cloned into pTLN (Lorenz *et al*, 1996). For the surface expression assay (below), an HA epitope was inserted between residues E168 and K169 (extra-cytosolic loop between helices B and C) of hClC-7. Point mutations were introduced by PCR. For the G796fs mutation of hClC-7, the 3'UTR until the new stop codon was added. All constructs were confirmed by sequencing the complete ORF.

Primary antibodies were mouse anti-LAMP-1, -LAMP-2 (both DSHB; clones H4A3 and H4B4, respectively) and -HA epitope (Covance, clone HA.11), rat anti-HA epitope (Roche, clone 3F10) and rabbit anti-ClC-7 (7N4B (Kornak *et al*, 2001)). Secondary antibodies conjugated to AlexaFluor 488, 546 or 633 were from Molecular Probes, HRP-conjugated antibodies from Jackson ImmunoResearch.

Voltage clamp, qualitative pH_i determinations and surface expression assay in *Xenopus laevis* oocytes. *Xenopus laevis* oocytes were injected with cRNA (23 ng for ClC-7 constructs and additional 23 ng for Ostm1 or Ostm1/CD4

chimeras) which was transcribed with the mMessage Machine kit (Ambion) from pTLN (Lorenz *et al*, 1996). After three days incubation at 17°C, currents were measured using standard two-electrode voltage clamp (TEVC) employing TurboTEC amplifiers (npi electronic) and pClamp10.2 software (Molecular Devices). Measurements were performed at room temperature or, when specified, the temperature was regulated by a TC-344 Heater Controller (Warner). Oocytes were superfused with modified ND96 saline (96 mM NaCl, 2 mM K-gluconate, 1.8 mM Ca-gluconate, 1 mM Mg-gluconate). pH was buffered with 5 mM HEPES, Tris, MES or 10 mM phosphate as appropriate. Ion substitutions were done by replacing NaCl with equimolar amounts of $NaNO_3$, NaI, NaBr or Na-gluconate. Proton transport activity was measured qualitatively by recording intracellular pH (pH_i) changes exploiting the pH-sensitive fluorescence of BCECF (injected 10-30 min prior to the experiment) in the Fluorocyte (Zdebik *et al*, 2008). ClC-7/Ostm1 was activated by an extended depolarization to +80 mV for 10 s followed by 3 s hyperpolarization to -80 mV, with a holding potential of -30 mV using TEVC. Currents and fluorescence changes were recorded simultaneously with the pClamp10.2 software.

To determine the temperature-dependence of activation rate constants $R = 1/\tau$ of ClC-7^{PM}/Ostm1, only the first 250 ms of depolarization (+80 mV) were fitted to an exponential function, because we observed a slow component at 37°C that significantly adds to the activation at later times. This was also observed with uninjected oocytes. Q_{10} values were determined by $Q_{10} = (R_2/R_1)^{10/(T_2-T_1)}$, with R_1 and R_2 being the activation rate constants at temperatures T_1 (37°C) and T_2 (21°C), respectively.

Surface expression of HA-tagged ClC-7 protein was determined 3 days after cRNA injection by an immuno-chemiluminescence assay as described (Zerangue *et al*, 1999) with up to 20 oocytes per construct and experiment.

Patch-clamp experiments. Whole-cell patch-clamp measurements on cultured cells used patch pipettes of 3-5 MΩ resistance were filled with (in mM) 110 CsCl, 10 NaCl, 0.5 $CaCl_2$, 1 EGTA, 2 MgATP, 40 HEPES, pH 7.2. The calculated free

Ca^{++} concentration was 180 nM. The bath solution contained (in mM) 130 NaCl, 5 KCl, 1 $MgCl_2$, 1 $CaCl_2$, 10 glucose, 20 HEPES, pH 7.4 with NaOH. Osmolarity was adjusted with sucrose to 280-290 mosmol/l for the pipette solution and to 300 mosmol/l for the extracellular solution. To alter Cl^- and pH gradients, NaCl was replaced partially by Na-gluconate and pH was buffered with 20 mM Tris (pH 8.4) or 20 mM MES (pH 6.4). Data were acquired with an EPC-10 double amplifier and Pulse software (HEKA).

Tail current analysis. To measure 'open exchanger' currents, activation pulses of 1 s to +80 mV were applied followed by 500-ms test voltage steps of 20 mV from -100 to +100 mV. To determine reversal potentials, the length and voltage of the activation pulse were adjusted to yield similarly strong current amplitudes at different $[Cl^-]_o$ and pH_o values. Activation pulses were preceded by 'control pulses' of 50 ms to -80, -40 and 0 mV to estimate background currents and their reversal potentials. Test pulses were applied in 20-mV steps between 0 and +40 or -20 and +20 mV. Reversal potentials of background currents ($E_{rev,bg}$) and of tail currents ($E_{rev,meas}$) were determined by intrapolation. Reversal potentials of ClC-7^{PM}/Ostm1 ($E_{rev,ClC-7}$) were then calculated by

$$E_{rev,ClC-7} = (E_{rev,meas} – (E_{rev,bg} * (\gamma_{bg}/\gamma_{tot}))) / (1 – (\gamma_{bg}/\gamma_{tot}))$$

(where γ_{bg} is the background slope conductance and γ_{tot} is the total slope conductance at the test pulses) and corrected for liquid-junction potentials. The equation

$$E_{rev} = -(RT/(m+n)F)* \ln (([Cl]_o^m * [H]_i^n) / ([Cl]_i^m * [H]_o^n))$$

(where R,T and F have the usual meaning) was used for reversal potential calculation for an mCl^-/nH^+-exchanger with different coupling ratios of m:n.

To determine the voltage dependence of gating, we transfected HeLa cells with human ClC-7^{PM}(R762Q) and Ostm1-GFP. Adding GFP to the C-terminus of Ostm1 did not change currents, but selecting for fluorescent cells increased the success rate of patch-clamping. Fits of mono-exponential functions to tail currents measured as in Figure 3C gave currents at the time of the voltage step. These values were corrected by subtracting mean currents of non-transfected

cells at +80 mV (the test voltage). These corrected currents were normalized to currents at +140 mV, and normalized currents were averaged from 5 experiments. These data were fitted to a Boltzmann function of the form:

$f(V) = 1/(1 + \exp(z_n * e_0(V_{½} - V)/kT))$,

with e_0 being the elementary charge, V the voltage, k the Boltzmann constant and T the temperature, to yield $V_{½}$ (the voltage for half-maximal activation) and z_n (the gating charge (or valence)). Apparent p_{open} (Figure 3D) was obtained by normalization to obtain p_{open}= 1 for $V \rightarrow \infty$.

Cell culture and immunofluorescence microscopy. Plasmid DNA encoding the respective construct(s) was transfected into HeLa or tsA201 cells using FuGENE6 (Roche). Cells were grown at 37°C for 24 to 48 h before patch-clamp experiments or fixation with 4% PFA in PBS for 15 min. For immunolabelling, cells were incubated with 30 mM glycine in PBS for 5 min and permeabilized with 0.1 % saponin in PBS for 10 min. Both primary and AlexaFluor-coupled secondary antibodies were applied in PBS/0.05% saponin supplemented with 3 % BSA. Images were acquired with an LSM510 laser scanning confocal microscope equipped with a 63x 1.4 NA oil-immersion lens (Zeiss).

To evaluate ClC-7-dependent trafficking of Ostm1/CD4 chimeras to late endosomes/lysosomes, GFP-tagged chimeras were assayed by co-localization of GFP fluorescence with LAMP-1 immuno-labelling. For double-transfected cells, only those cells in which rClC-7-HA co-localized with LAMP-1 were considered. More than 100 cells were counted per construct and experiment. 3-4 independent experiments were performed per construct, with the investigator blinded to the kind of chimera.

References

Accardi A, Miller C (2004) Secondary active transport mediated by a prokaryotic homologue of ClC Cl^- channels. *Nature* **427:** 803-807

Accardi A, Pusch M (2000) Fast and slow gating relaxations in the muscle chloride channel CLC-1. *J Gen Physiol* **116:** 433-444

Bauer CK, Steinmeyer K, Schwarz JR, Jentsch TJ (1991) Completely functional double-barreled chloride channel expressed from a single *Torpedo* cDNA. *Proc Natl Acad Sci U S A* **88:** 11052-11056

Bennetts B, Roberts ML, Bretag AH, Rychkov GY (2001) Temperature dependence of human muscle ClC-1 chloride channel. *J Physiol* **535:** 83-93.

Bergsdorf EY, Zdebik AA, Jentsch TJ (2009) Residues important for nitrate/proton coupling in plant and mammalian CLC transporters. *J Biol Chem* **284:** 11184-11193

Bykova EA, Zhang XD, Chen TY, Zheng J (2006) Large movement in the C terminus of CLC-0 chloride channel during slow gating. *Nat Struct Mol Biol* **13:** 1115-1119

Chalhoub N, Benachenhou N, Rajapurohitam V, Pata M, Ferron M, Frattini A, Villa A, Vacher J (2003) Grey-lethal mutation induces severe malignant autosomal recessive osteopetrosis in mouse and human. *Nat Med* **9:** 399-406

Cleiren E, Benichou O, Van Hul E, Gram J, Bollerslev J, Singer FR, Beaverson K, Aledo A, Whyte MP, Yoneyama T, deVernejoul MC, Van Hul W (2001) Albers-Schönberg disease (autosomal dominant osteopetrosis, type II) results from mutations in the *ClCN7* chloride channel gene. *Hum Mol Genet* **10:** 2861-2867

de Santiago JA, Nehrke K, Arreola J (2005) Quantitative Analysis of the Voltage-dependent Gating of Mouse Parotid ClC-2 Chloride Channel. *J Gen Physiol* **126:** 591-603

Diewald L, Rupp J, Dreger M, Hucho F, Gillen C, Nawrath H (2002) Activation by acidic pH of CLC-7 expressed in oocytes from *Xenopus laevis*. *Biochem Biophys Res Commun* **291:** 421-424.

Dutzler R, Campbell EB, Cadene M, Chait BT, MacKinnon R (2002) X-ray structure of a ClC chloride channel at 3.0 Å reveals the molecular basis of anion selectivity. *Nature* **415:** 287-294

Dutzler R, Campbell EB, MacKinnon R (2003) Gating the selectivity filter in ClC chloride channels. *Science* **300:** 108-112

Estévez R, Boettger T, Stein V, Birkenhäger R, Otto M, Hildebrandt F, Jentsch TJ (2001) Barttin is a Cl^--channel β-subunit crucial for renal Cl^--reabsorption and inner ear K^+-secretion. *Nature* **414:** 558-561

Estévez R, Pusch M, Ferrer-Costa C, Orozco M, Jentsch TJ (2004) Functional and structural conservation of CBS domains from CLC chloride channels. *J Physiol* **557:** 363-378

Feng L, Campbell EB, Hsiung Y, MacKinnon R (2010) Structure of a eukaryotic CLC transporter defines an intermediate state in the transport cycle. *Science* **330:** 635-641

Fong P, Rehfeldt A, Jentsch TJ (1998) Determinants of slow gating in ClC-0, the voltage-gated chloride channel of *Torpedo marmorata*. *Am J Physiol* **274:** C966-C973

Frattini A, Pangrazio A, Susani L, Sobacchi C, Mirolo M, Abinun M, Andolina M, Flanagan A, Horwitz EM, Mihci E, Notarangelo LD, Ramenghi U, Teti A, Van Hove J, Vujic D, Young T, Albertini A, Orchard PJ, Vezzoni P, Villa A (2003) Chloride channel *ClCN7* mutations are responsible for severe recessive, dominant, and intermediate osteopetrosis. *J Bone Miner Res* **18:** 1740-1747

Friedrich T, Breiderhoff T, Jentsch TJ (1999) Mutational analysis demonstrates that ClC-4 and ClC-5 directly mediate plasma membrane currents. *J Biol Chem* **274:** 896-902

Graves AR, Curran PK, Smith CL, Mindell JA (2008) The Cl^-/H^+ antiporter ClC-7 is the primary chloride permeation pathway in lysosomes. *Nature* **453:** 788-792

Hanke W, Miller C (1983) Single chloride channels from *Torpedo* electroplax. Activation by protons. *J Gen Physiol* **82:** 25-45.

Hebeisen S, Heidtmann H, Cosmelli D, González C, Poser B, Latorre R, Alvarez O, Fahlke C (2003) Anion permeation in human ClC-4 channels. *Biophys J* **84:** 2306-2318.

Jentsch TJ (2007) Chloride and the endosomal-lysosomal pathway: emerging roles of CLC chloride transporters. *J Physiol* **578:** 633-640

Jentsch TJ (2008) CLC chloride channels and transporters: From genes to protein structure, pathology and physiology. *Crit Rev Biochem Mol Biol* **43:** 3-36

Jentsch TJ, Stein V, Weinreich F, Zdebik AA (2002) Molecular structure and physiological function of chloride channels. *Physiol Rev* **82:** 503-568.

Jentsch TJ, Steinmeyer K, Schwarz G (1990) Primary structure of *Torpedo marmorata* chloride channel isolated by expression cloning in *Xenopus* oocytes. *Nature* **348:** 510-514

Kasper D, Planells-Cases R, Fuhrmann JC, Scheel O, Zeitz O, Ruether K, Schmitt A, Poët M, Steinfeld R, Schweizer M, Kornak U, Jentsch TJ (2005) Loss of the chloride

channel ClC-7 leads to lysosomal storage disease and neurodegeneration. *EMBO J* **24:** 1079-1091

Kornak U, Kasper D, Bösl MR, Kaiser E, Schweizer M, Schulz A, Friedrich W, Delling G, Jentsch TJ (2001) Loss of the ClC-7 chloride channel leads to osteopetrosis in mice and man. *Cell* **104:** 205-215

Lange PF, Wartosch L, Jentsch TJ, Fuhrmann JC (2006) ClC-7 requires Ostm1 as a β-subunit to support bone resorption and lysosomal function. *Nature* **440:** 220-223

Letizia C, Taranta A, Migliaccio S, Caliumi C, Diacinti D, Delfini E, D'Erasmo E, Iacobini M, Roggini M, Albagha OM, Ralston SH, Teti A (2004) Type II benign osteopetrosis (Albers-Schönberg disease) caused by a novel mutation in *CLCN7* presenting with unusual clinical manifestations. *Calcified tissue international* **74:** 42-46

Li X, Wang T, Zhao Z, Weinman SA (2002) The ClC-3 chloride channel promotes acidification of lysosomes in CHO-K1 and Huh-7 cells. *Am J Physiol Cell Physiol* **282:** C1483-C1491.

Lisal J, Maduke M (2008) The ClC-0 chloride channel is a 'broken' Cl^-/H^+ antiporter. *Nat Struct Mol Biol* **15:** 805-810

Lloyd SE, Pearce SH, Fisher SE, Steinmeyer K, Schwappach B, Scheinman SJ, Harding B, Bolino A, Devoto M, Goodyer P, Rigden SP, Wrong O, Jentsch TJ, Craig IW, Thakker RV (1996) A common molecular basis for three inherited kidney stone diseases. *Nature* **379:** 445-449

Lorenz C, Pusch M, Jentsch TJ (1996) Heteromultimeric CLC chloride channels with novel properties. *Proc Natl Acad Sci U S A* **93:** 13362-13366

Ludewig U, Pusch M, Jentsch TJ (1996) Two physically distinct pores in the dimeric ClC-0 chloride channel. *Nature* **383:** 340-343

Markovic S, Dutzler R (2007) The structure of the cytoplasmic domain of the chloride channel ClC-Ka reveals a conserved interaction interface. *Structure* **15:** 715-725

Matsuda JJ, Filali MS, Volk KA, Collins MM, Moreland JG, Lamb FS (2008) Overexpression of ClC-3 in HEK293T cells yields novel currents that are pH-dependent. *Am J Physiol Cell Physiol* **294:** C251-C262

Meyer S, Dutzler R (2006) Crystal structure of the cytoplasmic domain of the chloride channel ClC-0. *Structure* **14:** 299-307

Meyer S, Savaresi S, Forster IC, Dutzler R (2007) Nucleotide recognition by the cytoplasmic domain of the human chloride transporter ClC-5. *Nat Struct Mol Biol* **14:** 60-67

Middleton RE, Pheasant DJ, Miller C (1996) Homodimeric architecture of a ClC-type chloride ion channel. *Nature* **383:** 337-340

Miller C, White MM (1984) Dimeric structure of single chloride channels from Torpedo electroplax. *Proc Natl Acad Sci U S A* **81:** 2772-2775

Neagoe I, Stauber T, Fidzinski P, Bergsdorf EY, Jentsch TJ (2010) The late endosomal CLC-6 mediates proton/chloride countertransport in heterologous plasma membrane expression. *J Biol Chem* **285:** 21689-21697

Nguitragool W, Miller C (2006) Uncoupling of a CLC Cl^-/H^+ exchange transporter by polyatomic anions. *J Mol Biol* **362:** 682-690

Novarino G, Weinert S, Rickheit G, Jentsch TJ (2010) Endosomal chloride-proton exchange rather than chloride conductance is crucial for renal endocytosis. *Science* **328:** 1398-1401

Orhan G, Fahlke C, Alekov AK (2011) Anion- and Proton-Dependent Gating of ClC-4 Anion/Proton Transporter under Uncoupling Conditions. *Biophys J* **100:** 1233-1241

Pangrazio A, Pusch M, Caldana E, Frattini A, Lanino E, Tamhankar PM, Phadke S, Lopez AG, Orchard P, Mihci E, Abinun M, Wright M, Vettenranta K, Bariae I, Melis D, Tezcan I, Baumann C, Locatelli F, Zecca M, Horwitz E, Mansour LS, Van Roij M, Vezzoni P, Villa A, Sobacchi C (2010) Molecular and clinical heterogeneity in *CLCN7*-dependent osteopetrosis: report of 20 novel mutations. *Hum Mutat* **31:** E1071-1080

Phadke SR, Fischer B, Gupta N, Ranganath P, Kabra M, Kornak U (2010) Novel mutations in Indian patients with autosomal recessive infantile malignant osteopetrosis. *The Indian journal of medical research* **131:** 508-514

Picollo A, Malvezzi M, Accardi A (2010) Proton block of the CLC-5 Cl^-/H^+ exchanger. *J Gen Physiol* **135:** 653-659

Picollo A, Malvezzi M, Houtman JC, Accardi A (2009) Basis of substrate binding and conservation of selectivity in the CLC family of channels and transporters. *Nat Struct Mol Biol* **16:** 1294-1301

Picollo A, Pusch M (2005) Chloride / proton antiporter activity of mammalian CLC proteins ClC-4 and ClC-5. *Nature* **436:** 420-423

Piwon N, Günther W, Schwake M, Bösl MR, Jentsch TJ (2000) ClC-5 Cl^--channel disruption impairs endocytosis in a mouse model for Dent's disease. *Nature* **408:** 369-373

Pressey SN, O'Donnell KJ, Stauber T, Fuhrmann JC, Tyynelä J, Jentsch TJ, Cooper JD (2010) Distinct neuropathologic phenotypes after disrupting the chloride transport

proteins ClC-6 or ClC-7/Ostm1. *Journal of neuropathology and experimental neurology* **69:** 1228-1246

Pusch M, Ludewig U, Jentsch TJ (1997) Temperature dependence of fast and slow gating relaxations of ClC-0 chloride channels. *J Gen Physiol* **109:** 105-116

Pusch M, Ludewig U, Rehfeldt A, Jentsch TJ (1995) Gating of the voltage-dependent chloride channel ClC-0 by the permeant anion. *Nature* **373:** 527-531

Pusch M, Steinmeyer K, Jentsch TJ (1994) Low single channel conductance of the major skeletal muscle chloride channel, ClC-1. *Biophys J* **66:** 149-152

Robertson JL, Kolmakova-Partensky L, Miller C (2010) Design, function and structure of a monomeric ClC transporter. *Nature* **468:** 844-847

Scheel O, Zdebik A, Lourdel S, Jentsch TJ (2005) Voltage-dependent electrogenic chloride proton exchange by endosomal CLC proteins. *Nature* **436:** 424-427

Scholl U, Hebeisen S, Janssen AG, Müller-Newen G, Alekov A, Fahlke C (2006) Barttin modulates trafficking and function of ClC-K channels. *Proc Natl Acad Sci U S A* **103:** 11411-11416

Schulz P, Werner J, Stauber T, Henriksen K, Fendler K (2010) The G215R mutation in the Cl^-/H^+-antiporter ClC-7 found in ADO II osteopetrosis does not abolish function but causes a severe trafficking defect. *PLoS One* **5:** e12585

Smith AJ, Lippiat JD (2010) Voltage-dependent charge movement associated with activation of the CLC-5 $2Cl^-/1H^+$ exchanger. *FASEB J* **24:** 3696-3705

Stauber T, Jentsch TJ (2010) Sorting motifs of the endosomal/lysosomal CLC chloride transporters. *J Biol Chem* **285:** 34537-34548

Steinmeyer K, Schwappach B, Bens M, Vandewalle A, Jentsch TJ (1995) Cloning and functional expression of rat CLC-5, a chloride channel related to kidney disease. *J Biol Chem* **270:** 31172-31177

Tajima M, Hayama A, Rai T, Sasaki S, Uchida S (2007) Barttin binds to the outer lateral surface of the ClC-K2 chloride channel. *Biochem Biophys Res Commun* **362:** 858-864

Waguespack SG, Koller DL, White KE, Fishburn T, Carn G, Buckwalter KA, Johnson M, Kocisko M, Evans WE, Foroud T, Econs MJ (2003) Chloride channel 7 (*CLCN7*) gene mutations and autosomal dominant osteopetrosis, type II. *J Bone Miner Res* **18:** 1513-1518

Wartosch L, Fuhrmann JC, Schweizer M, Stauber T, Jentsch TJ (2009) Lysosomal degradation of endocytosed proteins depends on the chloride transport protein ClC-7. *FASEB J* **23:** 4056-4068

Weinert S, Jabs S, Supanchart C, Schweizer M, Gimber N, Richter M, Rademann J, Stauber T, Kornak U, Jentsch TJ (2010) Lysosomal pathology and osteopetrosis upon loss of H^+-driven lysosomal Cl^- accumulation *Science* **328:** 1401-1403

Weinreich F, Jentsch TJ (2001) Pores formed by single subunits in mixed dimers of different CLC chloride channels. *J Biol Chem* **276:** 2347-2353

Zdebik AA, Zifarelli G, Bergsdorf E-Y, Soliani P, Scheel O, Jentsch TJ, Pusch M (2008) Determinants of anion-proton coupling in mammalian endosomal CLC proteins. *J Biol Chem* **283:** 4219-4227

Zerangue N, Schwappach B, Jan YN, Jan LY (1999) A new ER trafficking signal regulates the subunit stoichiometry of plasma membrane K_{ATP} channels. *Neuron* **22:** 537-548.

Zhang XD, Tseng PY, Chen TY (2008) ATP inhibition of CLC-1 is controlled by oxidation and reduction. *J Gen Physiol* **132:** 421-428

Zifarelli G, Pusch M (2009a) Conversion of the 2 Cl^-/1 H^+ antiporter ClC-5 in a NO_3^-/H^+ antiporter by a single point mutation. *EMBO J* **28:** 175-182

Zifarelli G, Pusch M (2009b) Intracellular regulation of human ClC-5 by adenine nucleotides. *EMBO Rep* **10:** 1111-1116

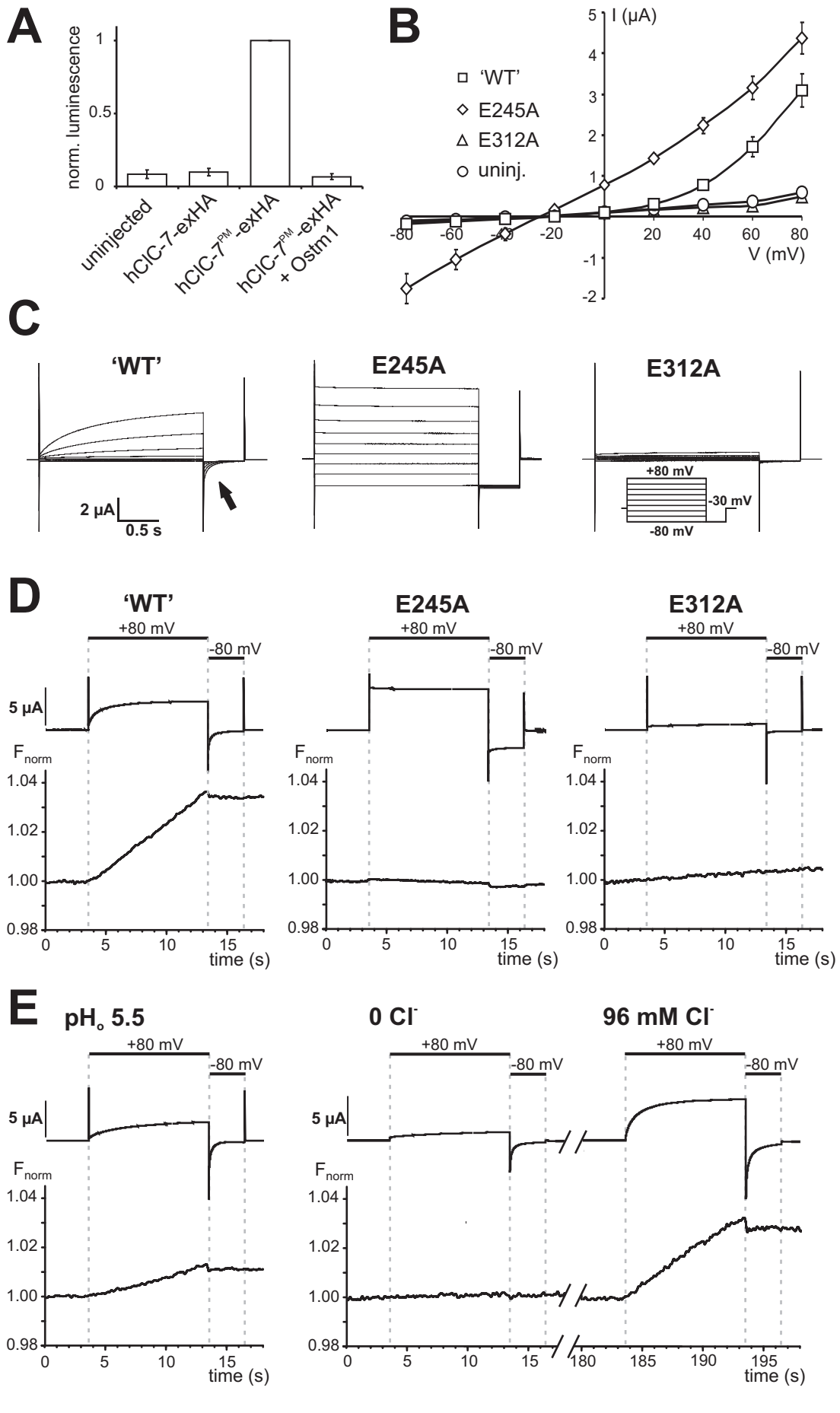
A
norm. luminescence
1
0.5
0
uninjected
hClC-7-exHA
hClC-7PM-exHA
hClC-7PM-exHA + Ostm1
B
I (μA)
'WT'
E245A
E312A
uninj.
V (mV)
C
'WT'
E245A
E312A
2 μA
0.5 s
+80 mV
-30 mV
-80 mV
D
'WT'
E245A
E312A
+80 mV
-80 mV
5 μA
Fnorm
time (s)
E
pHo 5.5
0 Cl-
96 mM Cl-
+80 mV
-80 mV
5 μA
Fnorm
time (s)

Figure 1

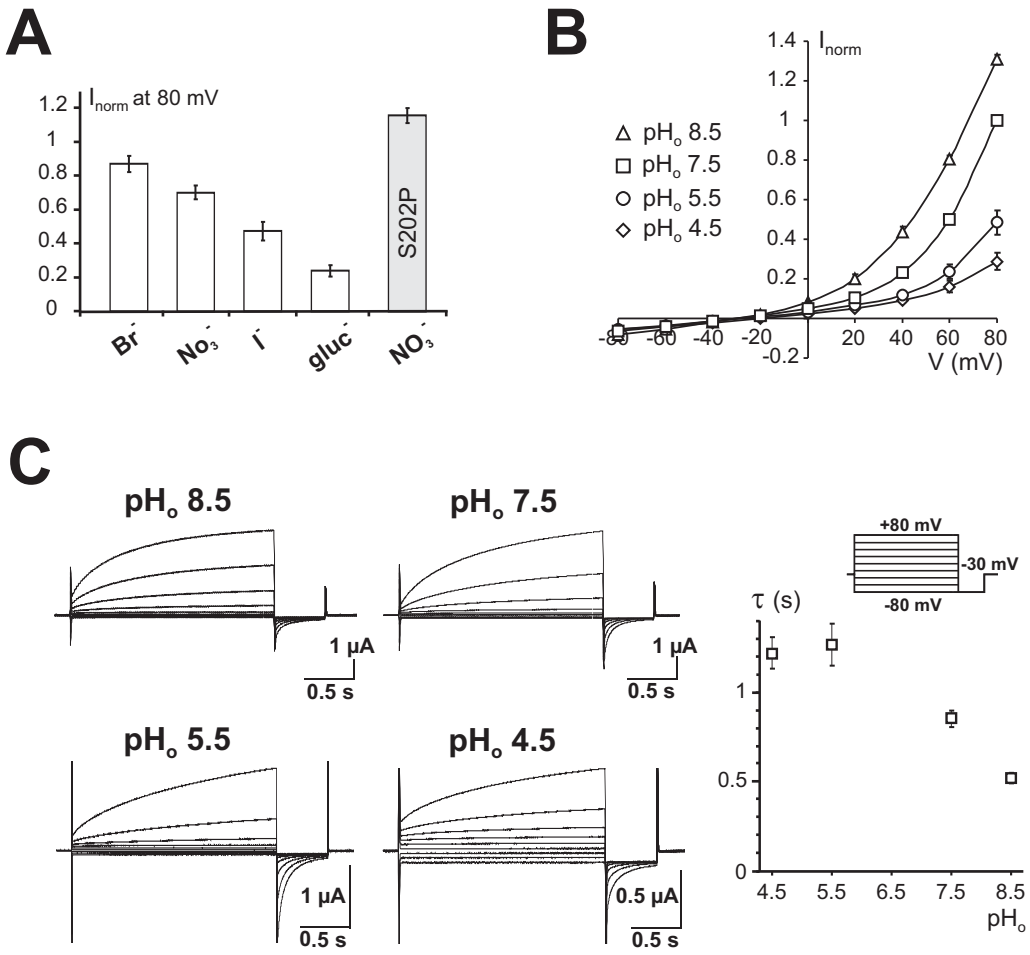
A
I_{norm} at 80 mV
1.2
1
0.8
0.6
0.4
0.2
0
S202P
Br⁻
NO_3^-
I⁻
gluc⁻
NO_3^-
B
I_{norm}
1.4
1.2
1
0.8
0.6
0.4
0.2
-0.2
pH_o 8.5
pH_o 7.5
pH_o 5.5
pH_o 4.5
-60
-40
-20
20
40
60
80
V (mV)
C
pH_o 8.5
pH_o 7.5
pH_o 5.5
pH_o 4.5
1 µA
0.5 s
1 µA
0.5 s
1 µA
0.5 s
0.5 µA
0.5 s
+80 mV
-30 mV
-80 mV
τ (s)
1
0.5
0
4.5
5.5
6.5
7.5
8.5
pH_o
D
21°C
29°C
37°C
2 µA
0.5 s

Figure 2

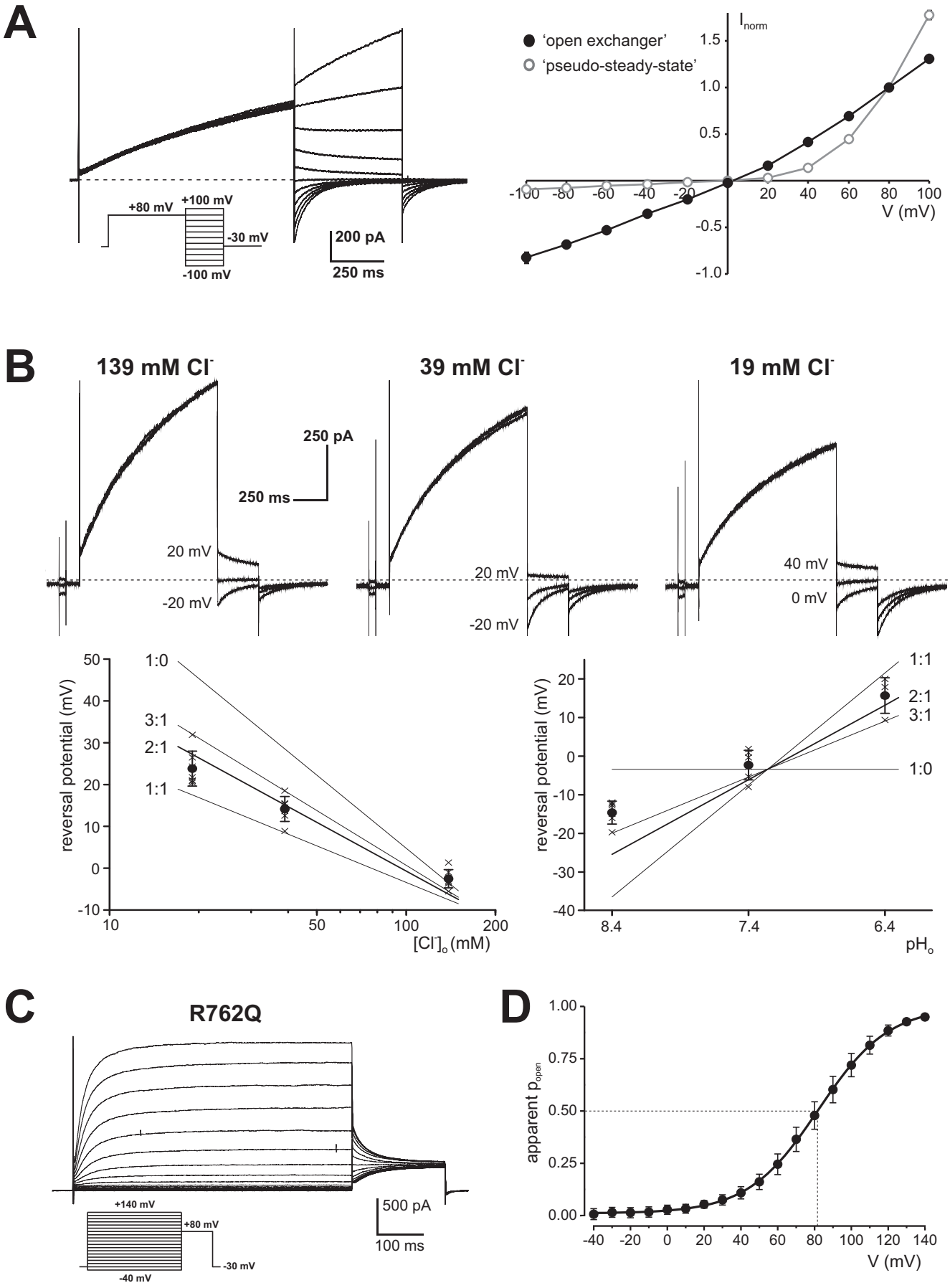
A
+80 mV
+100 mV
-30 mV
-100 mV
200 pA
250 ms
'open exchanger'
'pseudo-steady-state'
I_norm
V (mV)
B
139 mM Cl-
39 mM Cl-
19 mM Cl-
250 pA
250 ms
20 mV
-20 mV
40 mV
0 mV
reversal potential (mV)
[Cl-]o (mM)
pHo
1:0
3:1
2:1
1:1
C
R762Q
+140 mV
+80 mV
-30 mV
-40 mV
500 pA
100 ms
D
apparent popen
V (mV)

Figure 3

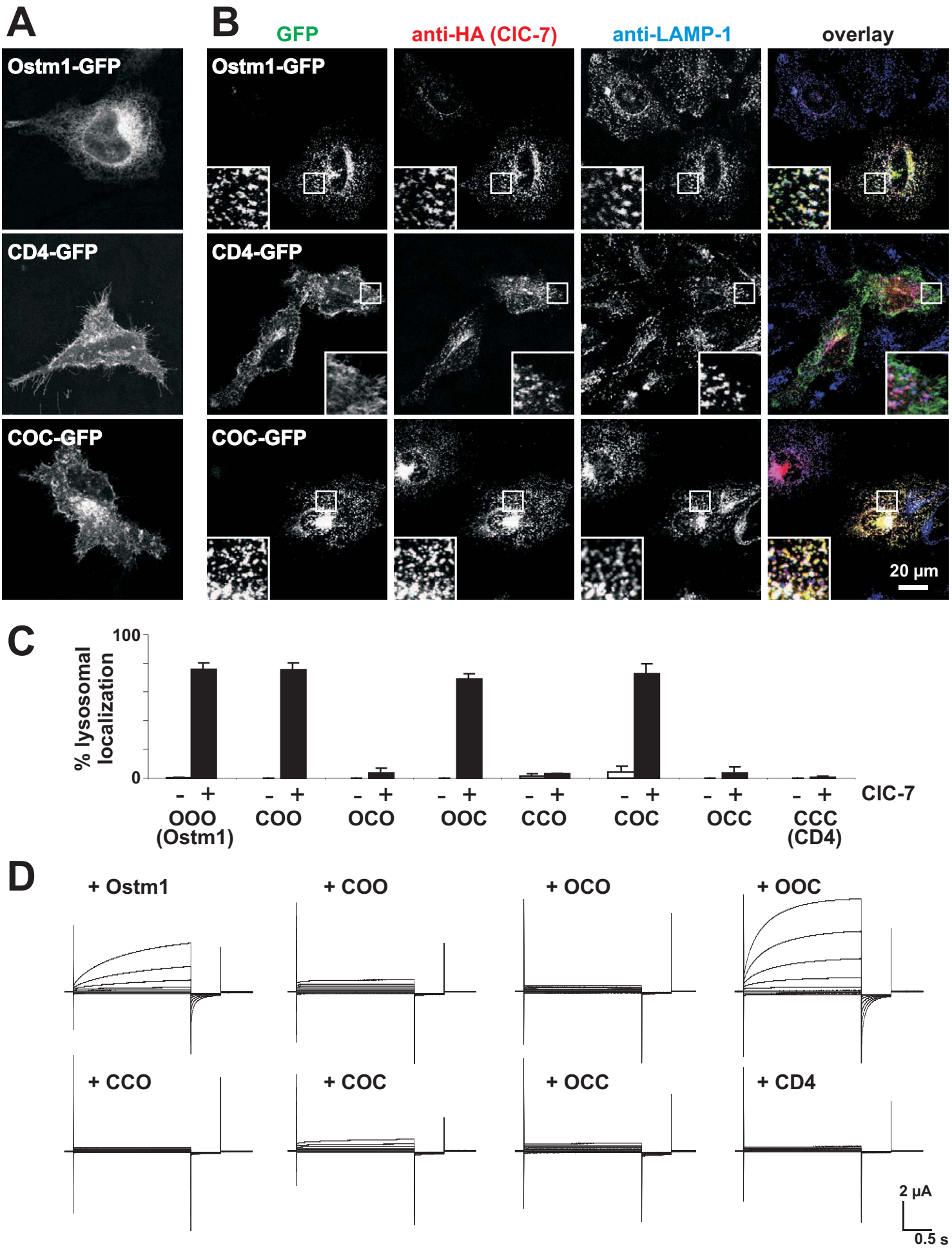
A
B
GFP
anti-HA (ClC-7)
anti-LAMP-1
overlay
Ostm1-GFP
CD4-GFP
COC-GFP
20 µm
C
% lysosomal localization
100
0
- + - + - + - + - + - + - + - +
ClC-7
OOO (Ostm1)
COO
OCO
OOC
CCO
COC
OCC
CCC (CD4)
D
+ Ostm1
+ COO
+ OCO
+ OOC
+ CCO
+ COC
+ OCC
+ CD4
2 µA
0.5 s

Figure 4

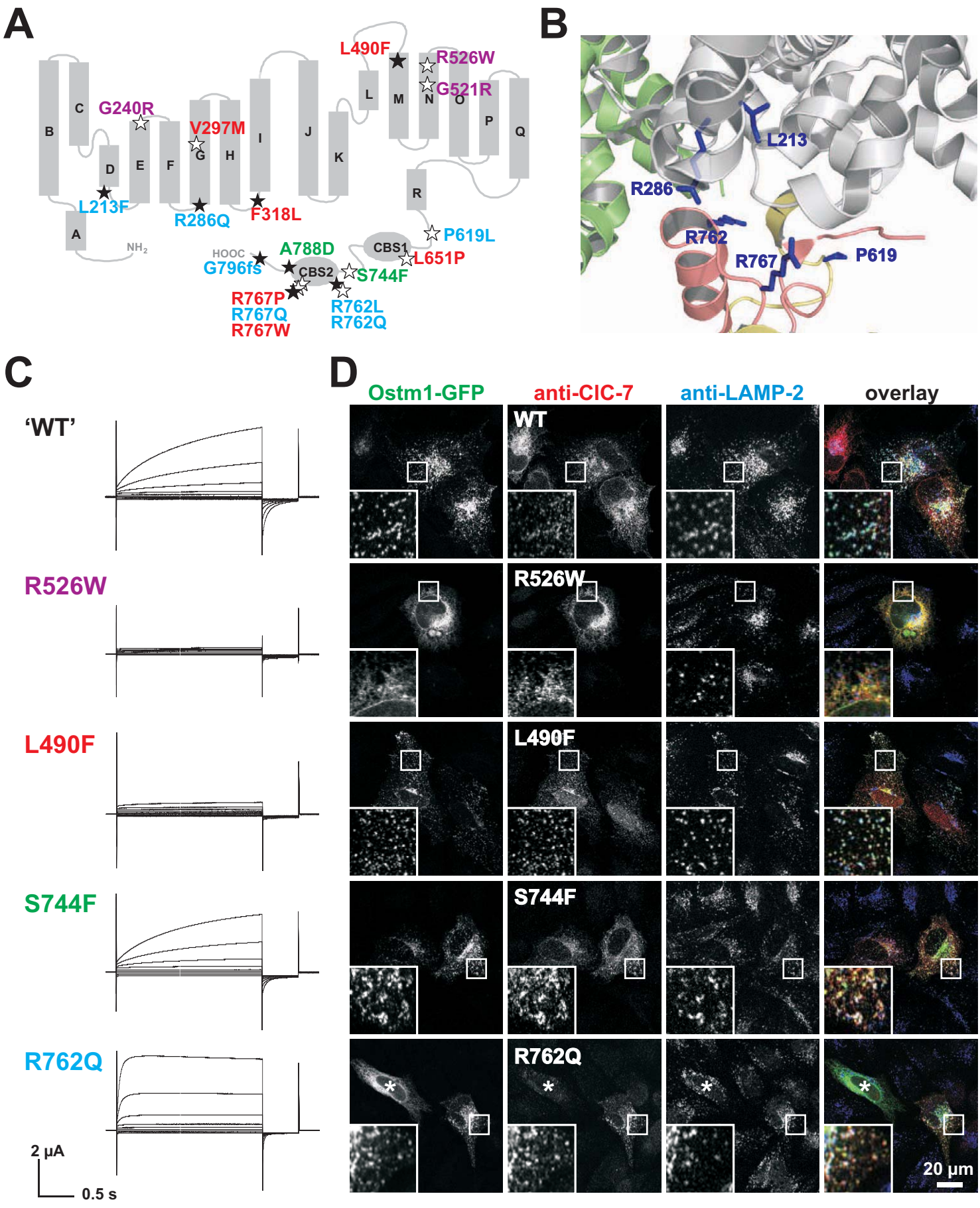
A
L490F
R526W
G521R
G240R
V297M
L213F
R286Q
F318L
P619L
A788D
G796fs
CBS1
L651P
CBS2
S744F
R767P
R767Q
R767W
R762L
R762Q
B
L213
R286
R762
R767
P619
C
'WT'
R526W
L490F
S744F
R762Q
2 µA
0.5 s
D
Ostm1-GFP
anti-CIC-7
anti-LAMP-2
overlay
WT
R526W
L490F
S744F
R762Q
20 µm

Figure 5

SUPPLEMENTARY INFORMATION TO

ClC-7 is a slowly voltage-gated $2Cl^-/1H^+$-exchanger and requires Ostm1 for transport activity

by

Lilia Leisle, Carmen F. Ludwig, Florian A. Wagner,
Thomas J. Jentsch and Tobias Stauber

SUPPLEMENTARY FIGURE LEGENDS

Supplementary Figure S1, related to Figure 1B,C and Figure 4: ClC-7^{PM}/Ostm1 currents in mammalian cells and *Xenopus* oocytes. (**A**) Representative current traces of hClC-7^{PM} ('WT'), hClC-7^{PM}(E247A) and hClC-7^{PM}(E314A) obtained with a voltage-clamp protocol consisting of 20mV steps to voltages between -80 and +80 mV for 2 s (inset) from oocytes three days after co-injection with Ostm1; as shown for rClC-7 in **Figure 1C**. (**B**) Typical whole-cell current traces (voltage-step protocol in inset) of rClC-7^{PM}/Ostm1 expressed in HeLa and tsA201 cells, respectively. Note pronounced tail currents with 121 mM Cl^- in the pipette solution. (**C**), Current-voltage curves (protocol as in (**B**)) of rClC-7^{PM} co-expressed with Ostm1-GFP in HeLa cells in the presence and absence, respectively, of 2 mM ATP in the pipette. Values are mean current densities ± s.e.m. of 9 (with ATP) and 8 (without ATP) cells. (**D**), Current-voltage curve (protocol as in (**B**)) of rClC-7^{PM} expressed with GFP or with Ostm1-GFP in HeLa cells. Non-transfected (n.t.) cells served as control. Mean current densities ± s.e.m. of 9 (rClC-7^{PM} co-expressed with Ostm1-GFP; same cells as in (**C**) in the presence of ATP), 12 (rClC-7^{PM} with GFP) and 10 (untransfected) cells.

Supplementary Figure S2, related to Figure 4A-C: Ostm1 domains needed for ClC-7-dependent trafficking to lysosomes. HeLa cells were transfected with the five C-terminally GFP-tagged Ostm1/CD4 chimeras (COO, OCO, OOC, CCO and OCC; C for CD4 and O for Ostm1; the position in the name indicates N-terminal, trans-membrane and C-terminal domain, respectively) that are not shown in **Figure 4A,B,** either alone (**A**) or with rClC-7-HA (**B**). Immunodetection as in **Figure 4**. Only Ostm1/CD4 chimeras containing the TMD of Ostm1 are carried to lysosomes.

Supplementary Figure S3, related to Figure 4D: Partial plasma membrane localization of rClC-7^{PM} irrespective of Ostm1/CD4 co-expression in HeLa cells. HeLa cells were co-transfected with rClC-7^{PM} and C-terminally GFP-tagged Ostm1/CD4 chimeras (three-letter code: C for CD4 and O for Ostm1; the position in the name indicates N-terminal, trans-

membrane and C-terminal domain, respectively), and immunostained after 30 h for ClC-7 and the lysosome marker protein LAMP-2. In all cases, rClC-7^{PM} was detected at the plasma membrane.

Supplementary Figure S4, related to Figure 5: Localization of amino acids mutated in osteopetrosis in CLC structure. X-ray structure of CmClC (Feng *et al*, 2010) displaying the location of the osteopetrosis-causing ClC-7 mutations analyzed in this study. The transmembrane core-forming parts of the two identical subunits are shown in gray, CBS1 in yellow and CBS2 in orange, using darker colors for one subunit. Positions in the structure are based on the published alignment (Feng *et al*, 2010) of ClC-7 with CmClC and are only shown in one subunit. Color code of mutants as in **Figure 5A**: purple, mutants that localize to the endoplasmic reticulum in hClC7/Ostm1; red, mutants showing no or strongly reduced currents in hClC-7^{PM}/Ostm1; green, mutants with WT-like currents; blue, mutants with accelerated activation kinetics.

Supplementary Figure S5, related to Figure 5: Analysis of additional *CLCN7* mutations found in human osteopetrosis. (**A**) Typical current traces of *Xenopus* oocytes co-expressing the indicated mutants (in hClC-7^{PM}) together with Ostm1. (**B**) Subcellular localization of the same mutant (but in hClC-7) upon co-expression with Ostm1-GFP in HeLa cells. Experiments were performed as in **Figure 5C,D**.

Supplementary Figure S6, related to Figure 5: Expression level of osteopetrosis-causing mutations that yielded no currents. (**A**) Immunoblot showing the protein expression of hClC-7^{PM} ('WT' or selected osteopetrosis-causing mutations, which yielded no currents upon expression in *Xenopus* oocytes but localized with Ostm1-GFP to lysosomes when expressed in the wildtype background in HeLa cells) three days after co-injection of the respective cRNA with that of Ostm1. Whole-oocyte protein equivalent to 1.5 oocytes was probed on immunoblot with rabbit antibody against ClC-7 (7N4B, Kornak et al., 2001) and mouse antibody against α-tubulin (clone DM1A, Sigma). Signal detection used chemiluminescence and

a camera system. (**B**) Signal intensities in immunoblots were quantified using the free software ImageJ and normalized to 'WT' after background subtraction. Mean values ± s.e.m. of three independent experiments are shown.

Supplementary Video 1, related to Figure 5B: Localization of 'accelerating' osteopetrosis mutations in the transmembrane-CBS interface.

Rotation by 15° of a close-up of X-ray structure of CmClC (Feng *et al*, 2010) seen from a different perspective as in **Figure 5B** to better visualize the proximity of ClC-7 residues that accelerate gating when mutated. The transmembrane part of one subunit is shown in light gray, CBS1 in yellow, and CBS2 in orange (or pink). Dark gray and red helices on the left correspond to transmembrane part and CBS2, respectively, of the attached second subunit of the homodimer.

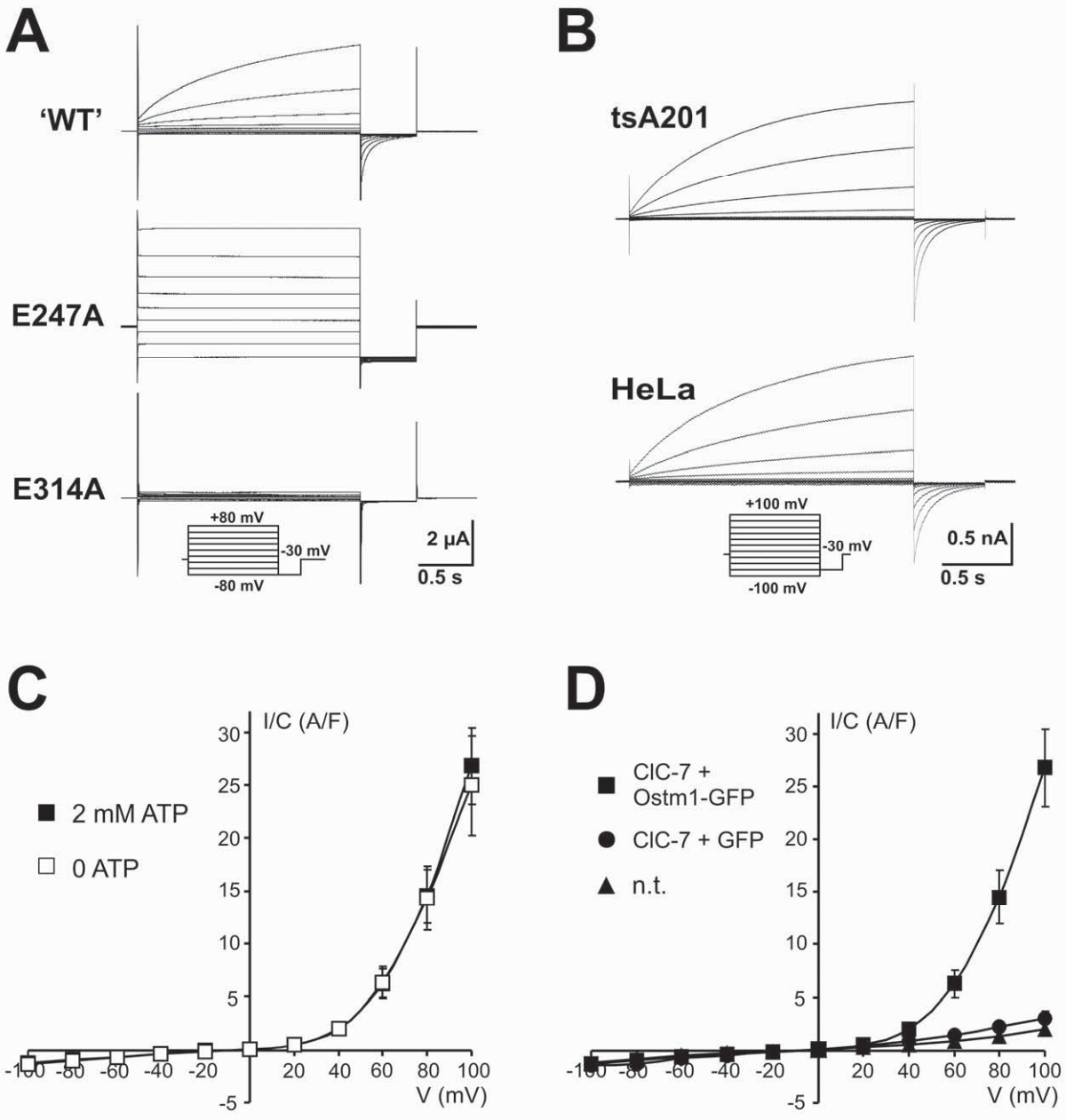

Supplementary Figure S1

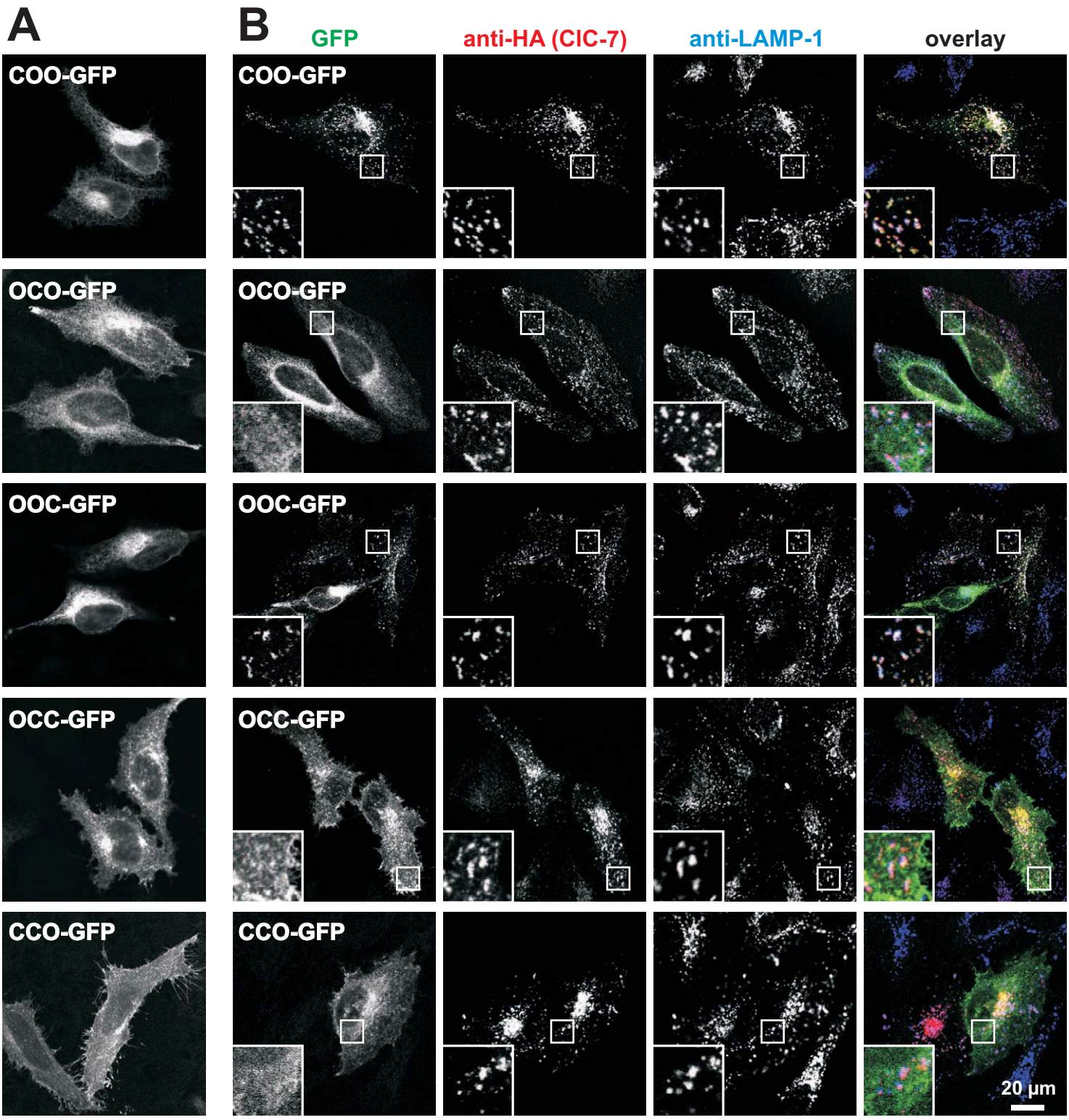

Supplementary Figure S2

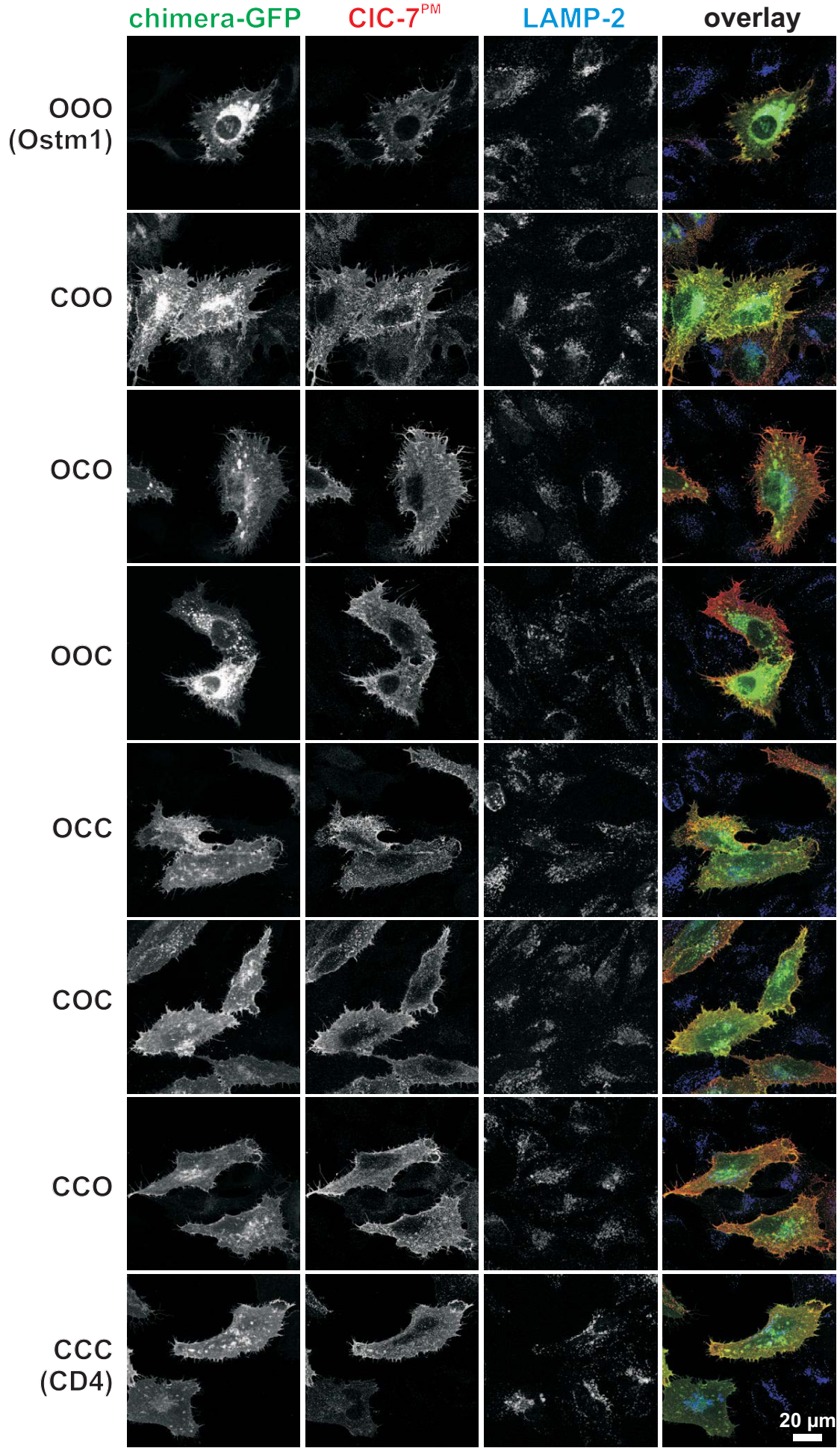

Supplementary Figure S3

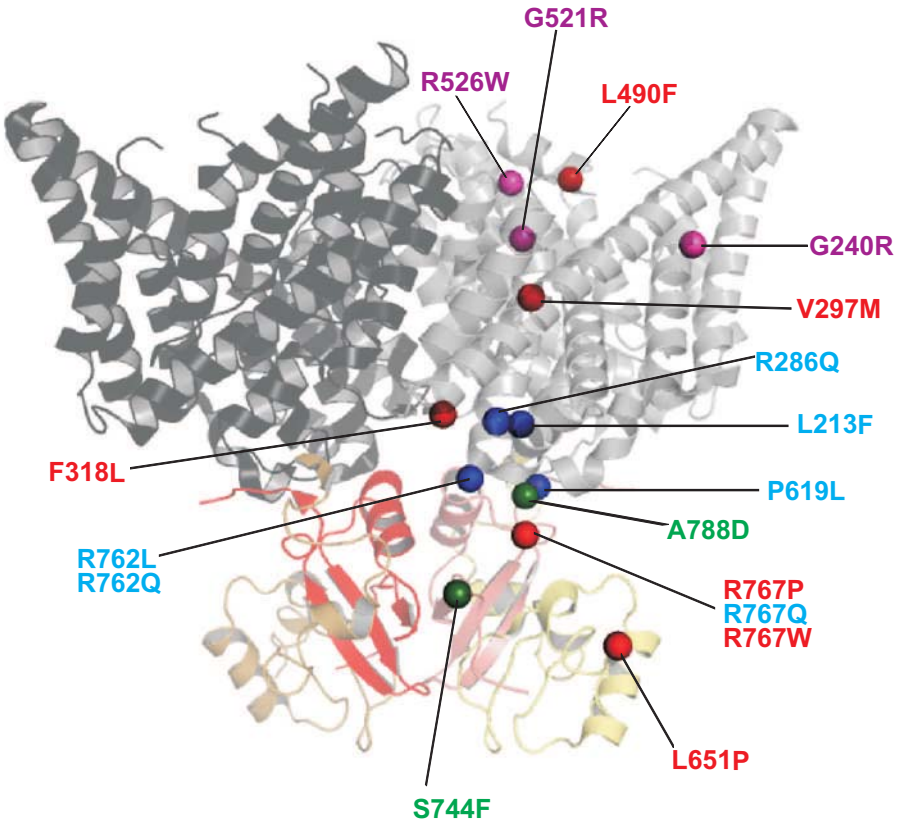

Supplementary Figure S4

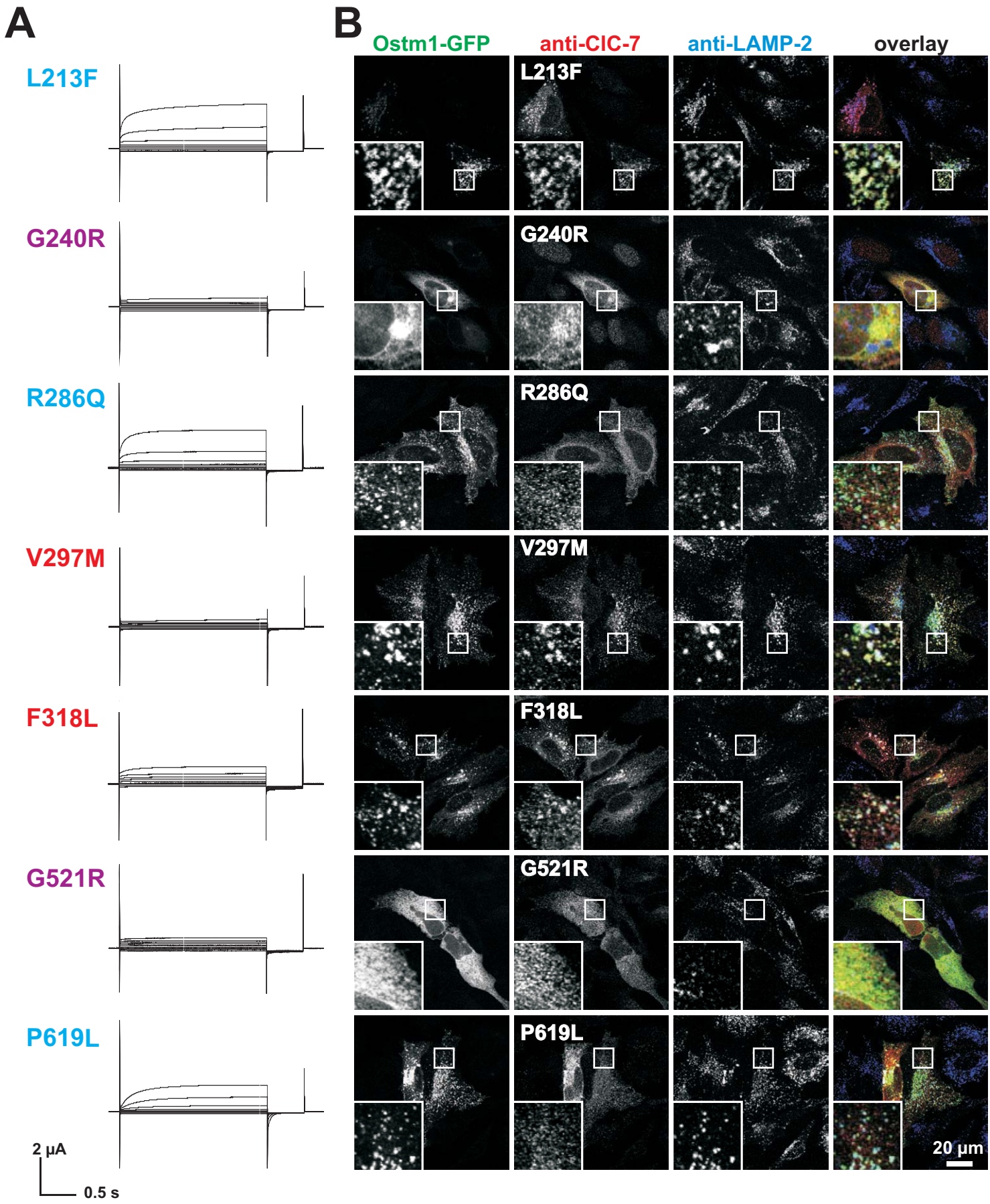

Supplementary Figure S5, part 1

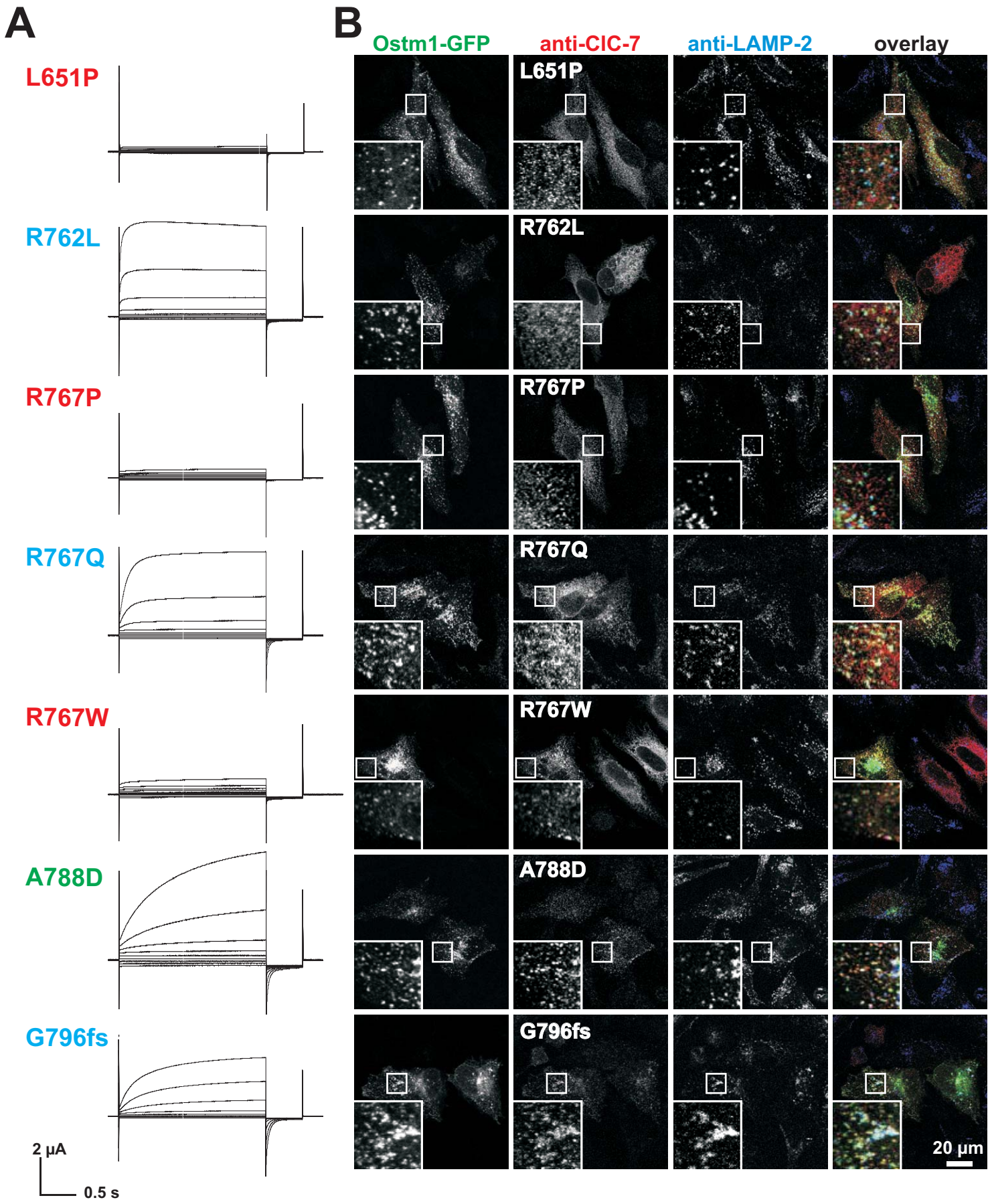

Supplementary Figure S5, part 2

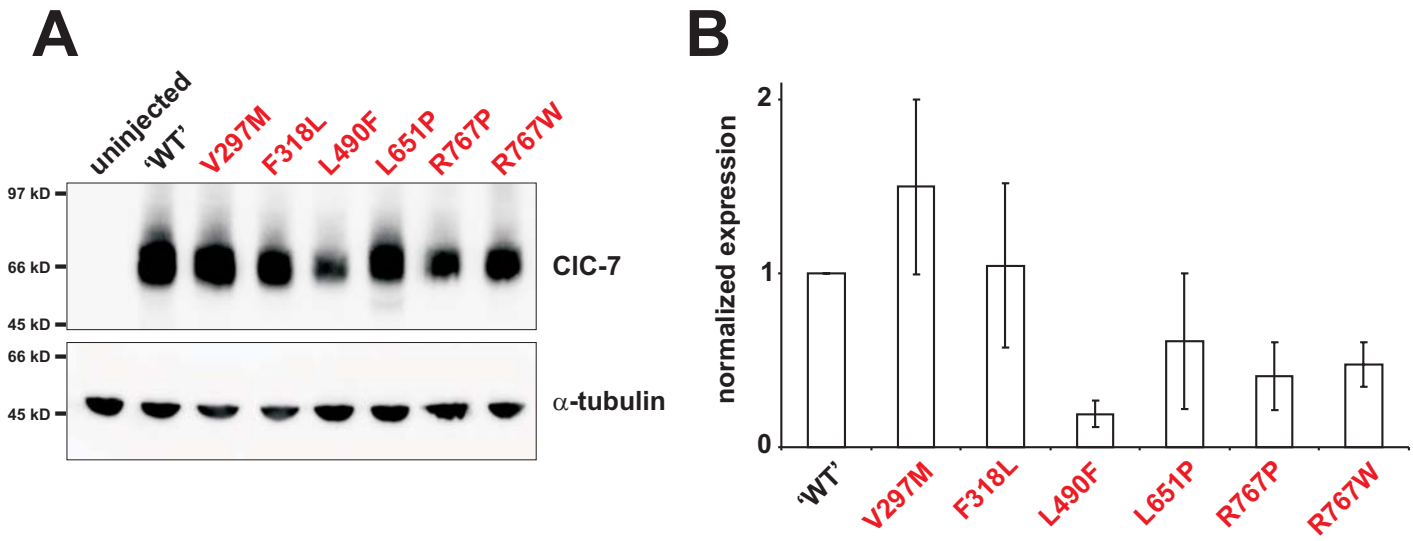

Supplementary Figure S6